

MIT Open Access Articles

Alignment of the CMS muon system with cosmic-ray and beam-halo muons

The MIT Faculty has made this article openly available. ***Please share*** how this access benefits you. Your story matters.

Citation	CMS Collaboration et al. "Alignment of the CMS muon system with cosmic-ray and beam-halo muons." Journal of Instrumentation, 5 (March 2010): T03020 © 2010 IOP Publishing Ltd and SISSA
As Published	http://dx.doi.org/10.1088/1748-0221/5/03/T03020
Publisher	IOP Publishing
Version	Author's final manuscript
Citable link	https://hdl.handle.net/1721.1/121593
Terms of Use	Creative Commons Attribution-Noncommercial-Share Alike
Detailed Terms	http://creativecommons.org/licenses/by-nc-sa/4.0/

Massachusetts Institute of Technology

DSpace@MIT

CMS Paper

2010/02/05

Alignment of the CMS Muon System with Cosmic-Ray and Beam-Halo Muons

The CMS Collaboration*

arXiv:0911.4022v2 [physics.ins-det] 8 Feb 2010

Abstract

The CMS muon system has been aligned using cosmic-ray muons collected in 2008 and beam-halo muons from the 2008 LHC circulating beam tests. After alignment, the resolution of the most sensitive coordinate is 80 microns for the relative positions of superlayers in the same barrel chamber and 270 microns for the relative positions of endcap chambers in the same ring structure. The resolution on the position of the central barrel chambers relative to the tracker is comprised between two extreme estimates, 200 and 700 microns, provided by two complementary studies. With minor modifications, the alignment procedures can be applied using muons from LHC collisions, leading to additional significant improvements.

*See Appendix A for the list of collaboration members

1 Introduction

The primary goal of the Compact Muon Solenoid (CMS) experiment [1] is to explore particle physics at the TeV energy scale exploiting the proton-proton collisions delivered by the Large Hadron Collider (LHC) [2]. The CMS experiment features a large muon tracking system for identifying muons and reconstructing their momenta. As with all tracking systems, the momentum resolution of reconstructed tracks depends in part on the alignment of detector components in space: three translational and three rotational degrees of freedom for each component. The alignment procedure provides corrections to the relationships between local detector-bound coordinate frames and a single, global frame for all CMS tracking systems.

The muon system consists of hundreds of independent tracking chambers mounted within the CMS magnetic field return yoke. Three technologies are employed: Drift Tube (DT) chambers on the five modular wheels of the barrel section, Cathode Strip Chambers (CSC) on the six endcap disks (illustrated in Figs. 1 and 2) and Resistive Plate Chambers (RPC) throughout. The DTs and CSCs are sufficiently precise to contribute to the momentum resolution of high-momentum muons (several hundred GeV/c) assuming that these chambers are well-aligned relative to the CMS tracker, a one-meter radius silicon strip and pixel detector. Between the tracker and the muon system are electromagnetic and hadronic calorimeters (ECAL and HCAL, respectively) for particle identification and energy measurement, as well as the solenoid coil for producing an operating magnetic field strength of 3.8 T in which to measure charged-particle momenta (all shown in Fig. 1).

The CMS collaboration is developing multiple techniques to align the DT and CSC chambers and their internal layers. Photogrammetry and in-situ measurement devices [3] provide real-time monitoring of potential chamber movements on short timescales and measurements of degrees of freedom to which tracks are only weakly sensitive. Track-based alignment, the subject of this paper, optimizes component positions for a given set of tracks, directly relating the active elements of the detectors traversed by the charged particles in a shared coordinate frame. Methods using tracks are employed both to align nearby components relative to one another and to align all muon chambers relative to the tracker.

A challenge to track-based alignment in the CMS muon system is the presence of large quantities of material between the chambers. As a central design feature of the detector, 20–60 cm layers of steel are sandwiched between the chambers to concentrate the magnetic field and absorb beam-produced hadrons. Consequently, uncertainties in track trajectories become significant as muons propagate through the material, making it necessary to develop alignment procedures that are insensitive to scattering, even though typical deviations in the muon trajectories (3–8 mm) are large compared to the intrinsic spatial resolution (100–300 μm). Two types of approaches are presented in this paper: the relative alignment of nearby structures, which avoids extrapolation of tracks through material but does not relate distant coordinate frames to each other, and the alignment using tracks reconstructed in the tracker, which allows for a more sophisticated treatment of propagation effects by simplifying the interdependence of alignment parameters.

This paper begins with a brief overview of the geometry of the muon system and conventions to be used thereafter (Section 2), followed by presentations of three alignment procedures:

(a) internal alignment of layers within DT chambers using a combination of locally fitted track segments and survey measurements (Section 3);

(b) alignment of groups of overlapping CSC chambers relative to one another, using only

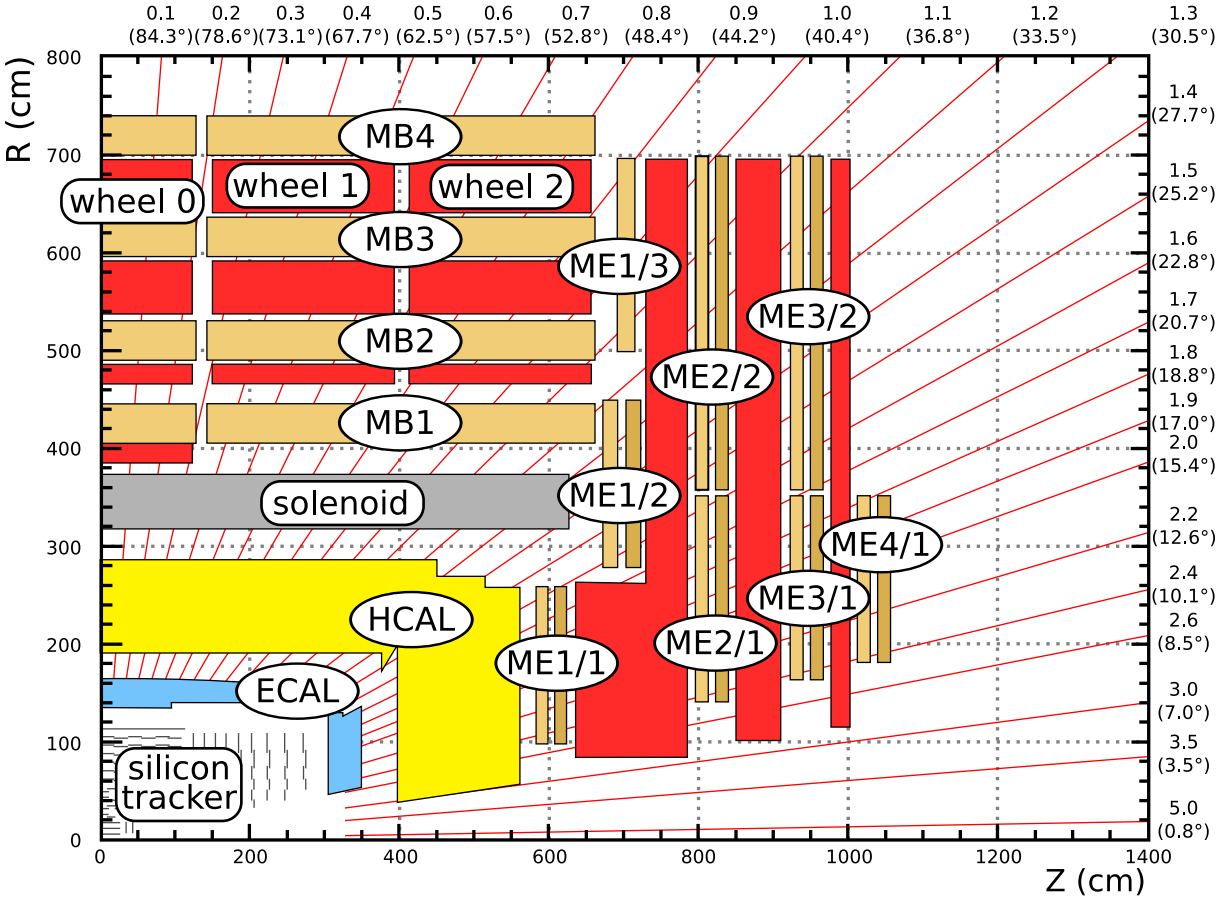

Figure 1: Quarter-view of CMS with labeled muon barrel (MB) and endcap (ME) stations. The steel yoke is represented by darkly shaded (red) blocks between the muon chambers. Pseudo-rapidities and polar angles are indicated on the top and right edges of the diagram.

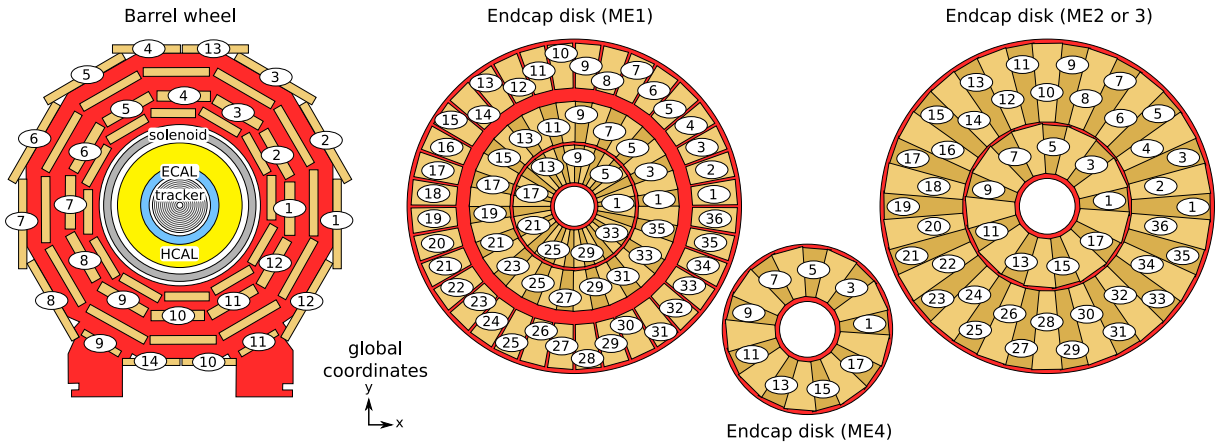

Figure 2: Transverse slices of CMS: the central barrel wheel and representative endcap disks, indicating the numbering of the DT azimuthal sectors in the barrel and the CSC chamber numbers in the endcaps.

locally fitted track segments (Section 4);

(c) alignment of each chamber relative to the tracker, using the tracks from the tracker, propagated to the muon system with a detailed map of the magnetic field and material distribution of CMS (Section 5).

Procedure (c), above, completes the alignment, relating all local coordinate frames to a shared frame. Its performance is greatly improved by supplying internally aligned chambers from procedure (a), such that only rigid-body transformations of whole chambers need to be considered. Procedures (b) and (c) both align CSC chambers relative to one another, but in different ways: (b) does not need many tracks, only about 1000 per chamber, to achieve high precision, and (c) additionally links the chambers to the tracker.

With the first LHC collisions, groups of CSCs will be interaligned using (b) and these rigid-body groups will be aligned relative to the tracker with (c). As more data become available, comparisons of results from (b) and (c) yield highly sensitive tests of systematic errors in (c).

Although the ideal tracks for these procedures are muons from LHC collisions, this paper focuses on application of the procedures using currently available data, namely cosmic rays (a and c) and beam-halo muons from circulating LHC beam tests in September 2008 (b). In particular, (c) requires a magnetic field to select high-quality, high-momentum muons and concurrent operation of the tracker and muon systems. The CMS Collaboration conducted a month-long data-taking exercise known as the Cosmic Run At Four Tesla (CRAFT) during October–November 2008, with the goal of commissioning the experiment for extended operation [4]. With all installed detector systems participating, CMS recorded 270 million cosmic-ray triggered events with the solenoid at its nominal axial field strength of 3.8 T. Due to geometric limitations imposed by the primarily vertical distribution of cosmic rays underground, (c) is performed with only a subset of DT chambers using CRAFT data, though the procedure will apply similarly to CSC chambers, once a large sample of inclined tracks becomes available.

The formalism and results of each procedure are presented together. Details of the data transfer and the computing model which were used to implement these procedures are described in Ref. [5].

2 Geometry of the Muon System and Definitions

Muon chambers are independent, modular track detectors, each containing 6–12 measurement layers, sufficient to determine the position and direction of a passing muon from the intersections of its trajectory with the layer planes ("hits"). The DT layers are oriented nearly perpendicular to lines radially projected from the beamline, and CSC layers are perpendicular to lines parallel with the beamline. Hits are initially expressed in a local coordinate frame (x, y, z) defined by the layers: $z = 0$ is the plane of the layer and x is the more precisely measured (or the only measured) of the two plane coordinates. On CSC layers, the most precise measurement is given by cathode strips, which fan radially from the beamline [6]. Defining "local $r\phi$" as the curvilinear coordinate orthogonal to the strips at all points, x and local $r\phi$ coincide only at the center of each CSC layer.

A semi-local coordinate system for the entire chamber is defined with x, y, and z axes nominally parallel to the layers' axes, but with a single origin. Within this common frame, the positions of hits from different layers can be related to each other and combined by a linear fit into segments with position $(\bar{x}, \bar{y})$ and direction $(\frac{\mathrm{d}x}{\mathrm{d}z}, \frac{\mathrm{d}y}{\mathrm{d}z})$. The nominal x direction of every chamber is perpendicular to the beamline and radial projections from the beamline.

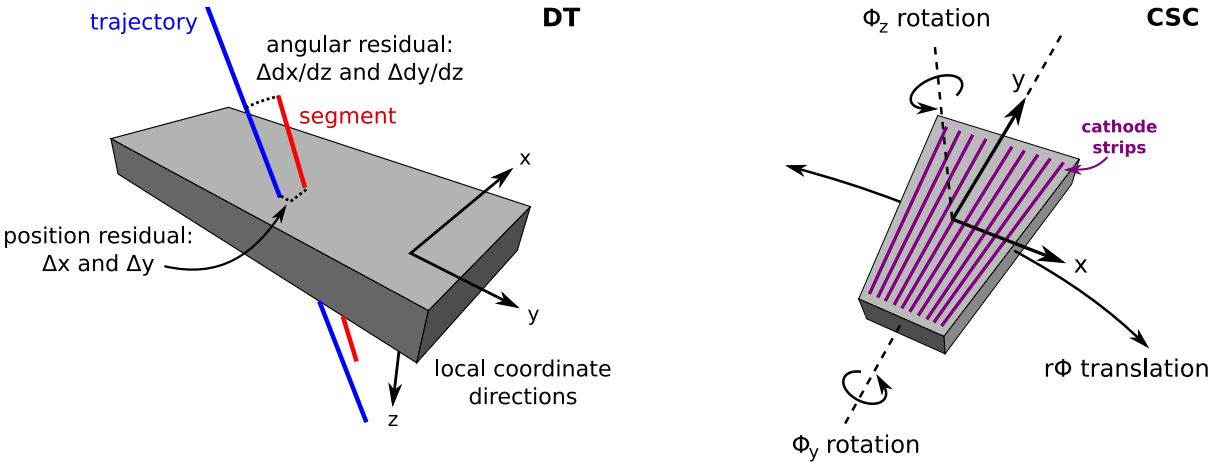

(a) (b)

Figure 3: (a) Coordinates and residuals for a DT chamber. (b) Coordinates and alignment parameters for a CSC chamber.

Residuals are differences between the predicted particle trajectories and the muon chamber data. Residuals can have as few as one component, from layers that measure only one dimension in the measurement plane, and as many as four components, Δx, Δy, $\Delta\frac{\mathrm{d}x}{\mathrm{d}z}$, $\Delta\frac{\mathrm{d}y}{\mathrm{d}z}$, from linear fits to all residuals in a chamber, as illustrated in Fig. 3(a).

To compare chamber positions to each other and to the position of the tracker, consider global coordinates (X, Y, Z) with the origin at the symmetry center of CMS, Z axis directed anticlockwise along the beamline, Y upward, and X horizontally toward the center of the LHC ring. Local coordinate systems are related to one another through an Alignment Integration Frame (AIF) that only approximates these global coordinates. It is not necessary to tightly control the definition of the AIF, as global translations and rotations of the whole system do not affect any physics measurements. Specific coordinate frames, at intermediate levels between layers and chambers and between chambers and global, are introduced in this paper as needed.

Corrections to positions and orientations of the layers and chambers are denoted as δ_x, δ_y, δ_z, δ_{ϕ_x}, δ_{ϕ_y}, and δ_{ϕ_z}, with x, y, and z expressed in local coordinates of the layer or chamber, and ϕ_x, ϕ_y, and ϕ_z as rotations around the corresponding axis; alignment corrections are small enough, $\mathcal{O}(\mathrm{mrad})$, to approximately commute. For CSC chambers, $\Delta(r\phi)$, $\Delta\frac{\mathrm{d}(r\phi)}{\mathrm{d}z}$, and $\delta_{r\phi}$ are more appropriate than Δx, $\Delta\frac{\mathrm{d}x}{\mathrm{d}z}$, and δ_x, respectively, to take advantage of the precision of the cathode strips. The most sensitive CSC alignment parameters are illustrated in Fig. 3(b).

DT layers are grouped into four-layer "superlayers," each of which measures one coordinate. Most DT chambers contain three superlayers, and the middle one, superlayer 2, is oriented a 90° angle with respect to superlayers 1 and 3 to measure y positions in the chamber coordinate frame. DT chambers farthest from the interaction point (MB4 in Fig. 1) contain only superlayers 1 and 3, and are therefore insensitive to y and $\frac{\mathrm{d}y}{\mathrm{d}z}$. CSC chambers contain six identical layers.

Chambers are grouped into "stations" by their distance from the interaction region, named MB1–MB4 in the barrel and ME$\pm$1/1, $\pm$1/2, $\pm$1/3, $\pm$2/1, $\pm$2/2, $\pm$3/1, $\pm$3/2, and $\pm$4/1 in the endcaps, labeled in Fig. 1. Azimuthal positions are called "sectors" in the barrel and simply "chamber number" in the endcaps, and these are labeled in Fig. 2.

3 Internal Alignment of DT Chambers

The layers and superlayers of DT chambers are aligned and analyzed in two steps. First, all layers in the chamber are aligned using a general Millepede algorithm [7], simultaneously optimizing alignment parameters and segment parameters, subject to constraints from a survey performed during construction. In the second step, the alignment of superlayers 1 and 3 are checked by fitting segments in each superlayer separately and measuring alignment errors from deviations between pairs of superlayer segments.

3.1 Layer Alignment

Measured trajectories within a single chamber do not suffer from uncertainties due to scattering in the steel between chambers. Segments, determined from linear fits to hits in one chamber only, are therefore used to determine the alignment of layers inside the chamber. The segment parameters depend on the layer alignment parameters within the chamber, so both must be resolved in a combined fit.

Without external constraints, the combined fit does not have a unique optimum, as it is insensitive to global distortions of the chamber. Consider a shear of the chamber that translates each layer in x by an amount proportional to its z position and an equal shear of all segment angles: this new geometry has exactly the same residuals as the unsheared geometry.

It is therefore necessary to add external survey measurements to constrain the fit; these are taken from two sources: (1) measurements of the wire end-pins taken during superlayer construction, and (2) photographs of reflective targets on the exterior of the superlayer ("photogrammetry"), taken during chamber construction. The averages of wire positions for all wires in each layer provide measurements of the x positions of the layers: RMS deviations from design geometry are 100 μm with 30–40 μm uncertainties. RMS deviations for the photogrammetry measurements are 200 μm in x and y, 500 μm in z, and 150 μrad in ϕ_x, ϕ_y, and ϕ_z.

The alignment of a tracking system subject to survey constraints can be expressed as the minimum of an objective function with terms derived from both tracks and survey. The objective function is

$$\chi^2 = \sum_i^{\text{layers}} \sum_j^{\text{tracks}} \left(\Delta\vec{x}_{ij} - A_j \cdot \vec{\delta}_i - B_i \cdot \delta\vec{p}_j\right)^T (\sigma_{\text{hit}}{}^2)_{ij}^{-1} \left(\Delta\vec{x}_{ij} - A_j \cdot \vec{\delta}_i - B_i \cdot \delta\vec{p}_j\right) + \sum_i^{\text{layers}} \sum_k^{\text{targets}} \left(\Delta\vec{\xi}_k - C_{ik} \cdot \vec{\delta}_i\right)^T (\sigma_{\text{survey}}{}^2)_k^{-1} \left(\Delta\vec{\xi}_k - C_{ik} \cdot \vec{\delta}_i\right) + \lambda \left|\sum_i^{\text{layers}} \vec{\delta}_i\right|^2 \quad , \quad (1)$$

where

- $\Delta\vec{x}_{ij}$ is the residual on layer i from track j (one-dimensional and in layer coordinates for the layer alignment case);
- $\vec{\delta}_i = (\delta_x, \delta_y, \delta_z, \delta_{\phi_x}, \delta_{\phi_y}, \delta_{\phi_z})$ is a vector of alignment corrections for layer i;
- $A_j = \begin{pmatrix} 1 & 0 & -\frac{dx}{dz}_j & -y_j\frac{dx}{dz}_j & x_j\frac{dx}{dz}_j & -y_j \end{pmatrix}$ is a 1×6 matrix transforming alignment parameter errors to residuals, dependent on the layer intersection (x_j, y_j) and entrance angle $\frac{dx}{dz}_j$ of track j;
- $\delta\vec{p}_j$ is a vector of corrections to the segment parameters;
- B_i is a matrix transforming variation of segment parameters into residuals on layer i (including a projection to the measured direction in the layer coordinate system);

- $({\sigma_{\text{hit}}}^2)^{-1}_{ij}$ is the inverse of the covariance matrix of the uncertainty in the hit on layer i, track j (single-valued in the layer alignment case);
- $\Delta\vec{\xi}_k$ is the difference between the nominal and measured position of survey target k;
- C_{ik} is a matrix transforming alignment errors in layer i to corrections in the position of survey target k;
- $({\sigma_{\text{survey}}}^2)^{-1}_k$ is the inverse of the covariance matrix of measurement k;
- $\lambda \left|\sum_i \vec{\delta}_i\right|^2$ is a Lagrange multiplier to inhibit translations and rotations of the chamber.

Segments are modeled as straight lines because the magnetic field is negligible inside the DT chambers. Survey targets from wire measurements are one-dimensional (the other two coordinates are given zero inverse uncertainties in $({\sigma_{\text{survey}}}^2)^{-1}_k$) and photogrammetry targets are included as individual survey constraints. Wire measurements apply only to relative positions of layers within their parent superlayer, and photogrammetry constraints apply to all layers in a superlayer as a group. This is expressed in $C_{ik} \cdot \vec{\delta}_i$ with terms such as $\vec{\delta}_i - [\vec{\delta}_1 + \vec{\delta}_2 + \vec{\delta}_3 + \vec{\delta}_4]/4$ to constrain layer i in a superlayer consisting of layers 1–4. Errors in survey measurements are assumed to be uncorrelated.

The χ^2 is quadratic in its parameters, so it is solved by the matrix inversion method. All layers were aligned in δ_x, δ_{ϕ_x}, δ_{ϕ_y}, and δ_{ϕ_z}, using about 20 000 cosmic ray tracks per chamber. The RMS of the corrections is 116 μm, 58 μrad, 63 μrad, and 49 μrad, respectively, and will be studied in more detail in the next section.

3.2 Test of Superlayer Alignment

To cross-check the alignment results in superlayers 1 and 3, the track-based data are compared with an independent set of photogrammetry measurements. The four hits in each superlayer define a superlayer segment with a one-dimensional position and slope, and segments from different superlayers must match at a common plane. Segment residuals, Δx_{S}, are the mismatch of these superlayer segments, and are sensitive to relative positions of the superlayers as well as their internal layer alignment parameters.

Segment residuals can be used to align superlayers 1 and 3 relative to one another without needing external constraints. The first term in Eq. (1) becomes

$$ {\chi_{\text{S}}}^2 = \sum_j^{\text{tracks}} \left[\Delta x_{\text{S}j} - \begin{pmatrix} 1 & -\frac{\mathrm{d}x}{\mathrm{d}z}_j & x_j \frac{\mathrm{d}x}{\mathrm{d}z}_j \end{pmatrix} \cdot \begin{pmatrix} \delta_{x_{\text{S}}} \\ \delta_{z_{\text{S}}} \\ \delta_{\phi_{y\text{S}}} \end{pmatrix} \right]^2 \frac{1}{(\sigma_{\Delta x_{\text{S}}})^2_j} \quad , \tag{2} $$

with no explicit dependence on track parameter corrections $\delta\vec{p}_j$. The minimization of Eq. (2) has a unique solution in $\delta_{x_{\text{S}}}$, $\delta_{z_{\text{S}}}$, and $\delta_{\phi_{y\text{S}}}$. It is not susceptible to shear, for example, because the slopes of the segments are fixed by the layers in each superlayer. Access to additional alignment parameters would require knowledge of y and $\frac{\mathrm{d}y}{\mathrm{d}z}$ which are not available in superlayers 1 and 3. The position of superlayer 2 cannot be determined in this way because it is the only y-measuring detector in a DT chamber.

To check the partially survey-based layer alignment from Section 3.1, segment residuals before and after layer alignment are plotted in Fig. 4(a). Each entry in the histogram is the mean of the Δx_{S} distribution for a single chamber. After layer alignment, segment positions and angles are more consistent between superlayers 1 and 3, leading to better matching at the common plane.

To verify the photogrammetry superlayer positions, $\delta_{x_{\text{S}}}$, $\delta_{z_{\text{S}}}$, and $\delta_{\phi_{y\text{S}}}$ from a minimization of

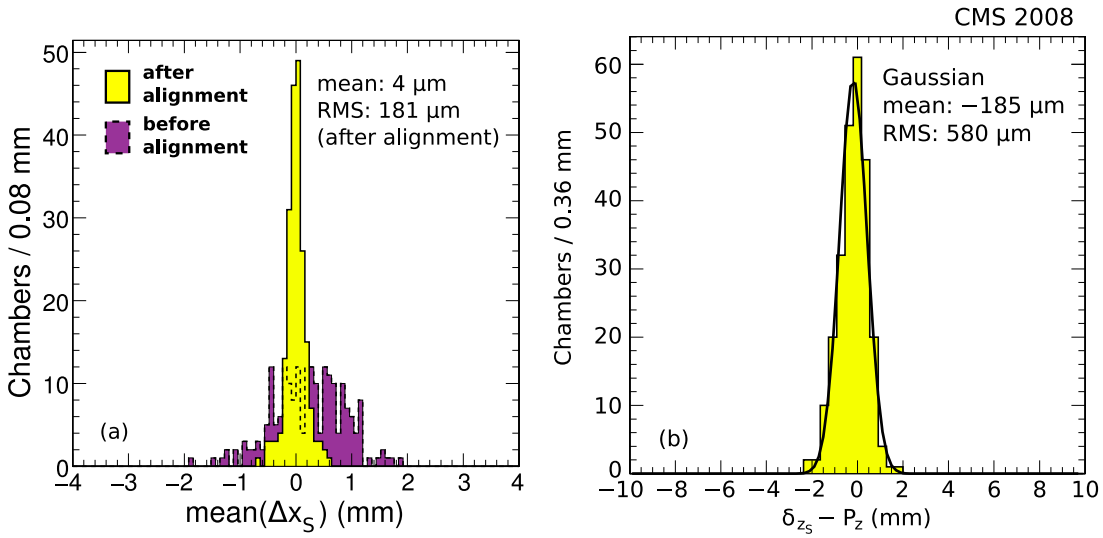

Figure 4: (a) Distribution of means of DT segment residuals for all chambers, before alignment presented in a dark/dashed histogram and after alignment in a light histogram. (b) Difference in z of superlayers as measured by tracks (δ_{z_S}) and photogrammetry (P_z).

Eq. (2) are directly compared with the photogrammetry measurements P_x, P_z, and P_{ϕ_y} of the relative superlayer positions. Figure 4(b) presents differences between the δ_{z_S} and P_z for each chamber. Typical values of δ_{z_S} are 1–1.5 mm due to a glue layer not included in the design geometry, and they agree with P_z on a per-chamber basis with 580 μm accuracy. Agreement of δ_{x_S} and $\delta_{\phi_{yS}}$ with P_x and P_{ϕ_y}, respectively, have 80 μm and 50 μrad accuracy. The segment measurements were applied to correct the internal geometry of the chambers.

4 Alignment of CSC Chambers in Rings

The CSC chambers in the muon endcaps were designed to overlap slightly along the edges of the sensitive area, such that muons passing through the narrow "overlap regions" would be observed by both of the neighboring chambers. This allows for a high-precision relative alignment of neighbors, and the relative measurements can be propagated around each ring of mutually overlapping chambers (illustrated in Fig. 2). All endcap rings are internally connected in this way except ME$\pm$1/3.

Although CSC chamber alignment using overlap tracks and alignment with tracks from the tracker (described in the next section) both determine the relative positions of CSC chambers, the overlap method has two advantages: (1) it achieves high precision with a small number of tracks, and (2) it is less prone to potential systematic errors in tracking. Since the two methods use different datasets in different ways, comparison between them can be used to diagnose systematic errors in tracks from the tracker or in their propagation to the muon endcaps. The disadvantage of the overlap alignment method is that it does not relate the ring coordinate frame to the AIF. A second alignment step is therefore necessary to align the whole ring as a rigid body relative to tracks from the tracker.

This section begins with a mathematical derivation of the algorithm, which is an analytic solution of Eq. (1) without external constraints, followed by an analysis of results from a Monte Carlo (MC) simulation and LHC single-beam tests. Cosmic ray results are not presented because the procedure requires forward-pointing tracks with approximate azimuthal symmetry.

4.1 Ring Alignment Algorithm

The basic strategy of CSC ring alignment is to fit segments from the same muon in each of the overlapping chambers independently and require them to match in position and slope for all chambers in the ring simultaneously. Segment parameters $\overline{r\phi}$ and $\frac{\mathrm{d}(r\phi)}{\mathrm{d}z}$ are computed using only cathode strips (the high-precision $r\phi$ coordinate), in a coordinate frame shared by pairs of chambers with $z = 0$ being the plane of symmetry between them. The curvature added to the segments by parameterizing them with a curvilinear coordinate is negligible. Chambers are labeled by indices i ranging from 1 to N ($N = 18$ or 36, depending on the ring), with the convention that $N + 1$ refers to chamber 1.

The general alignment objective function (see Eq. (1) for definitions) could be applied here, removing survey constraints and considering each track to consist of two "hits" with two components each: $\overline{r\phi}^{\,i}_j$ and $\frac{\mathrm{d}(r\phi)}{\mathrm{d}z}^{i}_{j}$. However, the geometry of this alignment case allows for simplifications which make the solution analytic. Overlap tracks only connect neighboring chambers, i and $i+1$, in such a way that residuals $\Delta(r\phi)^i_j = \overline{(r\phi)}^{\,i}_j - \overline{(r\phi)}^{\,i+1}_j$ and $\Delta\frac{\mathrm{d}(r\phi)}{\mathrm{d}z}^{i}_{j} = \frac{\mathrm{d}(r\phi)}{\mathrm{d}z}^{i}_{j} - \frac{\mathrm{d}(r\phi)}{\mathrm{d}z}^{i+1}_{j}$ constrain $A_j \cdot \left(\vec{\delta}^i - \vec{\delta}^{i+1}\right)$. Minimization of terms with the form

$$\begin{pmatrix} \Delta(r\phi)^i_j \\ \Delta\frac{\mathrm{d}(r\phi)}{\mathrm{d}z}^{i}_{j} \end{pmatrix} - A_j \cdot \left(\vec{\delta}^i - \vec{\delta}^{i+1}\right) \tag{3}$$

is functionally equivalent to Eq. (1) with $B_i \cdot \delta\vec{p}_j$ explicitly evaluated.

The overlap region is narrow in x and $\frac{\mathrm{d}x}{\mathrm{d}z}$ but wide in y, so three alignment parameters, $\delta_{r\phi}$, δ_{ϕ_y}, δ_{ϕ_z} can be accessed from these data (illustrated in Fig. 3(b)). The expression $A_j \cdot \left(\vec{\delta}^i - \vec{\delta}^{i+1}\right)$ expands to

$$\begin{pmatrix} 1 & 0 & -y_j \\ 0 & 1 & 0 \end{pmatrix} \begin{pmatrix} \delta^i_{r\phi} - \delta^{i+1}_{r\phi} \\ \delta^i_{\phi_y} - \delta^{i+1}_{\phi_y} \\ \delta^i_{\phi_z} - \delta^{i+1}_{\phi_z} \end{pmatrix} \quad . \tag{4}$$

Furthermore, correlations between $\delta^i_{\phi_y} - \delta^{i+1}_{\phi_y}$ and $\delta^i_{r\phi} - \delta^{i+1}_{r\phi}$ can be replaced with an order dependence. Rotating chambers (with segments following their orientation) to make segments parallel (ϕ_y alignment) would change their intercepts at $z = 0$, but translating chambers to make segments continuous at $z = 0$ ($r\phi$ alignment) would not change their slopes. If ϕ_y is aligned first and all segments are refitted, recomputing all residuals with the new geometry, a subsequent alignment of $r\phi$ (and ϕ_z) does not disturb the ϕ_y minimization. Therefore, two objective functions, ${\chi_1}^2$ and ${\chi_2}^2$, can be minimized separately as long as ${\chi_1}^2$ is optimized first, and the derived geometry is used to calculate quantities in ${\chi_2}^2$.

Putting all of this together,

$$\begin{aligned} {\chi_1}^2 &= \sum_{i}^{\text{chambers}} \sum_{j}^{\text{tracks}} \left[\Delta\frac{\mathrm{d}(r\phi)}{\mathrm{d}z}^{i}_{j} - \left(\delta^i_{\phi_y} - \delta^{i+1}_{\phi_y}\right)\right]^2 \frac{1}{({\sigma_{\frac{\mathrm{d}(r\phi)}{\mathrm{d}z}}}^2)^i_j} \\ {\chi_2}^2 &= \sum_{i}^{\text{chambers}} \sum_{j}^{\text{tracks}} \left[\Delta(r\phi)^i_j - \left(\delta^i_{r\phi} - \delta^{i+1}_{r\phi}\right) + y_j\left(\delta^i_{\phi_z} - \delta^{i+1}_{\phi_z}\right)\right]^2 \frac{1}{({\sigma_{r\phi}}^2)^i_j} \quad , \end{aligned} \tag{5}$$

where $({\sigma_{\frac{\mathrm{d}(r\phi)}{\mathrm{d}z}}}^2)^i_j$ and $({\sigma_{r\phi}}^2)^i_j$ are one-parameter errors in the residuals.

The sum over tracks in ${\chi_1}^2$ can be recognized as a weighted mean and the sum over tracks in ${\chi_2}^2$ as a linear fit of $\Delta(r\phi)^i_j$ versus y. Evaluating them (and introducing m, a, and b as functions returning the weighted mean, y intercept, and slope versus y of a given dataset, respectively), the objective functions can be replaced with

$$\begin{aligned} {\chi'_1}^2 &= \sum_i^{\text{chambers}} \left[m\left(\left\{\Delta\tfrac{\mathrm{d}(r\phi)}{\mathrm{d}z}^i_j\right\}\right) - \left(\delta^i_{\phi_y} - \delta^{i+1}_{\phi_y}\right)\right]^2 \\ {\chi'_{2a}}^2 &= \sum_i^{\text{chambers}} \left[a\left(\left\{\Delta(r\phi)^i_j, y_j\right\}\right) - \left(\delta^i_{r\phi} - \delta^{i+1}_{r\phi}\right)\right]^2 \\ {\chi'_{2b}}^2 &= \sum_i^{\text{chambers}} \left[b\left(\left\{\Delta(r\phi)^i_j, y_j\right\}\right) - \left(\delta^i_{\phi_z} - \delta^{i+1}_{\phi_z}\right)\right]^2 \quad , \end{aligned} \tag{6}$$

where ${\chi'_1}^2$ differs from ${\chi_1}^2$ by a constant factor and ${\chi'_{2a}}^2 + {\chi'_{2b}}^2$ differs from ${\chi_2}^2$ by a constant factor. To avoid rotations and twists of the whole ring, Lagrange multiplier $(\sum_i \delta^i_{\phi_y}/N)^2$ is added to ${\chi'_1}^2$, $(\sum_i \delta^i_{r\phi}/N)^2$ is added to ${\chi'_{2a}}^2$, and $(\sum_i \delta^i_{\phi_z}/N)^2$ is added to ${\chi'_{2b}}^2$, which favor solutions with minimal average corrections. Each of the three minimization problems has the same analytic solution, found by setting the derivatives of the objective function to zero and inverting the resulting $N \times N$ matrix of constants. This alignment method is applicable to any tracking system composed of a ring of pairwise overlapping detectors.

The method also enables three internal cross-checks; the following must be consistent with zero: $\sum_i a(\{\Delta(r\phi)^i_j, y_j\})$, $\sum_i b(\{\Delta(r\phi)^i_j, y_j\})$, and $\sum_i m(\{\Delta\frac{\mathrm{d}(r\phi)}{\mathrm{d}z}^i_j\})$. These closure tests are not sensitive to misalignments, but they determine whether the residuals are consistent with a closed loop. All three closure tests were found to be consistent with zero in these studies.

4.2 Monte Carlo Study

The procedure was applied to beam-halo events generated by Monte Carlo (based on a simulation described in Ref. [8]). The simulation has approximately the same number of events as the 2008 LHC dataset (33 000 tracks passing through the overlap regions of CSCs), but a different azimuthal and radial distribution. The distribution of beam-halo events is difficult to predict for a new accelerator, and in fact changed frequently during the first circulating beam tests. Since the alignment uncertainties are statistics-limited and the population of tracks in each chamber is only approximately the same as in data, the simulation provides only a rough guide for what to expect from the data.

From an initially misaligned detector, the procedure aligned δ_{ϕ_y} with 1.04 mrad accuracy (initially 2 mrad), $\delta_{r\phi}$ with 230 μm (initially 1000 μm), and δ_{ϕ_z} with 0.25 mrad (initially 1 mrad), determined from the RMS of differences between the aligned positions and the true positions of the chambers.

The second step, aligning the internally aligned rings relative to the tracker, was studied with a sample of simulated muons from proton collisions. It was found that 280 μm ring position accuracy in the X-Y plane can be achieved with 10 pb^{-1} of collisions. This second step cannot be applied with beam-halo muons because they generally do not cross both the muon chambers and the tracker.

4.3 Alignment Results

In September 2008, protons circulated in the LHC, producing beam-halo muons captured by CMS. The majority of the beam-halo data were collected from one 9-minute fill of the anti-

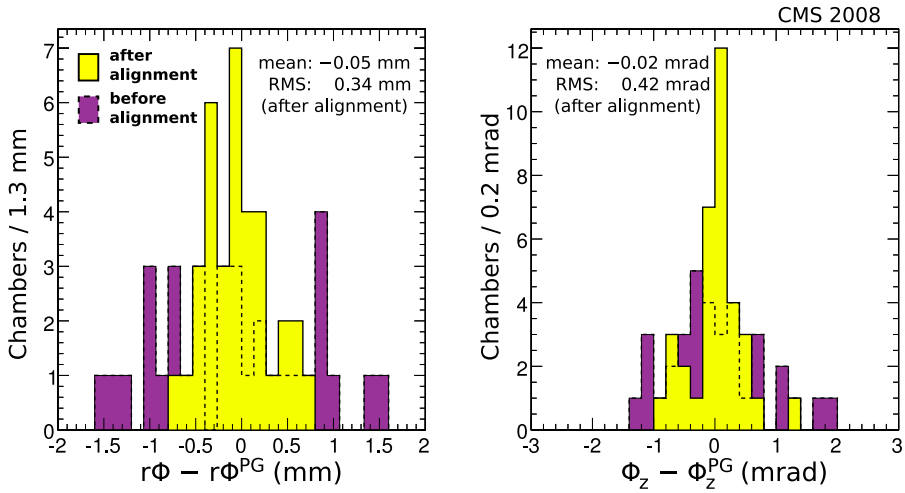

Figure 5: Difference between CSC positions and their photogrammetry measurements. Dark/dashed histograms are before alignment and light histograms are after alignment.

clockwise beam. More beam-halo muons illuminated the inner rings of the negative endcap because they tend to follow trajectories close to the beam-line and the anti-clockwise beam traverses CMS from the negative side. All chambers in ME$-2/1$ and ME$-3/1$ were operational, so these chambers were used to test the procedure.

Application of the alignment algorithm narrows the RMS of the $\Delta(r\phi)$ distribution from 1.42 to 0.98 mm. For comparison, the $\Delta(r\phi)$ distribution of the aligned simulation has an RMS of 1.12 mm.

To independently verify the results, they can be compared with photogrammetry measurements. The resolution in the positions of photogrammetry targets is 300 μm [9], which translates into resolutions of 210 μm and 0.23 mrad for $\delta_{r\phi}$ and δ_{ϕ_z} respectively. Photogrammetry measurements cannot determine δ_{ϕ_y} because the targets lie near the y axis of the chambers.

Figure 5 shows the difference between chamber coordinates and photogrammetry ($r\phi^{\mathrm{PG}}$ and ${\phi_z}^{\mathrm{PG}}$), before and after alignment. The RMS of these distributions after alignment, which are convolutions of photogrammetry errors and errors in the track-based measurements, are 340 μm and 0.42 mrad in $\delta_{r\phi}$ and δ_{ϕ_z} respectively. Subtracting the photogrammetry errors in quadrature, one can conclude that the track-based measurement has approximately 270 μm and 0.35 mrad uncertainties, in rough agreement with the prediction from simulation. In the absence of systematic uncertainties, several hours of similar beam-halo conditions would be sufficient to reduce the alignment error below the 170–200 μm intrinsic hit uncertainty for these chambers [6].

5 Alignment of DT Chambers in a Global Coordinate System

The muon alignment procedures presented in previous sections arrange layers and sets of chambers in self-consistent coordinate frames, but do not relate those frames to the other subsystems of CMS, in particular the tracker. In this section, a method is described to align muon chambers relative to the tracker by propagating the tracker tracks to the muon chambers. The method is equally applicable to DTs and CSCs, but cosmic rays only provide large numbers of tracks in the central region of the barrel.

Muons encounter significant scattering material between every two stations. With measure-

ments expressed as chamber residuals (Δx, Δy, $\Delta\frac{dx}{dz}$, $\Delta\frac{dy}{dz}$), this means there is a large component of random error in the trajectory between each measurement and the next. The residuals are therefore broadened beyond what would be expected from the intrinsic resolutions of the hits, but alignment information can be derived from the peak positions of those distributions.

In principle, muon chamber hits could be used in the track fits to narrow the distributions of residuals and improve the statistical precision of the alignment results. Including those hits biases the tracks, coupling track parameters and alignment parameters, thereby coupling alignment parameters of different chambers with each other. This coupling can be resolved by matrix inversion [7] or by reducing the weight of the muon chamber hits and iterating [10], but the structure of the probability distribution from scattering complicates these methods. Moreover, sufficient statistical precision can be achieved without muon chamber hits in the track fits (or equivalently, muon chamber hits with negligible weight in the fit).

This section describes muon chamber alignment using tracks determined purely by the tracker. Because the track parameters are not a function of the muon chamber positions, there is no mutual dependency to resolve, nor are the alignment parameters of different chambers coupled. However, the resulting chamber positions depend on the alignment of the tracker [11]: optimized muon chamber residuals does not guarantee that the combined tracker-muon system is globally undistorted. The first subsection below describes the algorithm with a discussion of propagation effects. Section 5.2 presents a Monte Carlo study of the procedure, and alignment results are presented in Sections 5.3 (residuals), 5.4 (cross-check), and 5.5 (momentum measurements). An alternative algorithm is under development to align muon chambers using matrix inversion; this is briefly described in Section 5.6.

5.1 The Reference-Target Algorithm

The "reference-target" algorithm divides the tracking volume into two regions: a "reference" (the tracker), in which normal track-fitting is performed, and a "target" (the muon chambers), in which unbiased residuals are computed from the propagated tracks. The simplicity this affords in the correlation matrix of alignment parameters allows more emphasis to be placed on the study of propagation effects.

The shape of the residuals distribution is fitted to a parameterized Ansatz function using an unbinned maximum likelihood method, rather than minimizing an objective function with a quadratic form like Eq. (1). This can be seen as a generalization of the standard method, because quadratic terms such as $(\Delta x_{ij} - A_j \cdot \vec{\delta}_i)^2/({\sigma_{\text{hit}}}^2)_{ij}$ are the logarithm of Gaussian likelihoods. Substituting a non-Gaussian Ansatz motivated by physical processes in track propagation introduces non-linearity to the derivative of the objective function which cannot be solved by matrix inversion. The non-linear minimization package MINUIT is used instead [12].

5.1.1 Propagation Effects

Residuals from propagated tracks can be affected by the following effects:

- misalignment (distributed as a δ-function in x, y, $\frac{dx}{dz}$, $\frac{dy}{dz}$ because it is strictly geometric);
- intrinsic hit resolution (negligible);
- statistical uncertainty in the fitted track parameters (Gaussian);
- hard Coulomb scattering off of nuclei (which has non-Gaussian tails);
- multiple Coulomb scattering (Gaussian in the limit of many interactions);
- background from pattern-recognition errors and noisy channels (non-Gaussian);

- systematic errors in magnetic field map and material budget for average energy loss (proportional to q/p_T and $q/|\vec{p}|^2$, respectively, where q, p_T, and $|\vec{p}|$ are the charge, transverse momentum, and magnitude of the momentum of the muon);
- systematic bias in the track source distribution (a function of the path of the track through the reference volume).

All but the last two effects are included in the Ansatz. The main non-Gaussian contribution is from events in which the muon interacts with a small number of nuclei, such that the distribution of deflections does not fully reach the Gaussian limit of the central limit theorem. There is no sharp distinction between single and multiple scattering, but it is sufficient to model the combined effect with a function having a Gaussian core and large tails, such as the tails of a Cauchy-Lorentz distribution. A smaller non-Gaussian contribution from pattern-recognition errors and noisy channels is also absorbed into the tails. The primary significance of the tails is to increase the likelihood of highly non-Gaussian residuals, and therefore stabilize the determination of the peak.

A magnetic field map resulting from detailed modeling and CRAFT data analysis [13] was used in this alignment, but the result is additionally verified by performing it separately with positively charged muons, negatively charged muons, and averaging the two. Magnetic field errors add contributions to residuals which are antisymmetric in charge, as do material budget errors because muons can only lose energy on average, and this deflects them in the direction of their curvature. Any charge-dependent effects from magnetic field map or material budget errors would cancel in the average. The RMS of differences with respect to not applying this averaging procedure are 100 μm in δ_x and 0.07 mrad in δ_{ϕ_y}, the two parameters most affected by magnetic field. These differences are small compared with other uncertainties.

The possibility of systematic bias in the track source has been addressed in the context of tracker alignment [14, 15] as weak modes in the procedure and has been studied in Ref. [11] for the tracker description used here. Any unresolved global distortions in the tracker would be extended to the muon system as well, though tracks would be guaranteed to match segments in the momentum range of the algorithm's application. The goal at this stage is to align muon chambers to the positions projected by the current best knowledge of the shape of the tracker.

5.1.2 The Alignment Ansatz Function

Misalignment offsets the peak of the residuals distribution, centering (Δx, Δy, $\Delta\frac{\mathrm{d}x}{\mathrm{d}z}$, $\Delta\frac{\mathrm{d}y}{\mathrm{d}z}$) at the values

$$\begin{pmatrix} \Delta x_0 \\ \Delta y_0 \\ \Delta\frac{\mathrm{d}x}{\mathrm{d}z}_0 \\ \Delta\frac{\mathrm{d}y}{\mathrm{d}z}_0 \end{pmatrix} = \begin{pmatrix} 1 & 0 & -\frac{\mathrm{d}x}{\mathrm{d}z} & -y\frac{\mathrm{d}x}{\mathrm{d}z} & x\frac{\mathrm{d}x}{\mathrm{d}z} & -y \\ 0 & 1 & -\frac{\mathrm{d}y}{\mathrm{d}z} & -y\frac{\mathrm{d}y}{\mathrm{d}z} & x\frac{\mathrm{d}y}{\mathrm{d}z} & x \\ 0 & 0 & 0 & -\frac{\mathrm{d}x}{\mathrm{d}z}\frac{\mathrm{d}y}{\mathrm{d}z} & 1+\left(\frac{\mathrm{d}x}{\mathrm{d}z}\right)^2 & -\frac{\mathrm{d}y}{\mathrm{d}z} \\ 0 & 0 & 0 & -1-\left(\frac{\mathrm{d}y}{\mathrm{d}z}\right)^2 & \frac{\mathrm{d}x}{\mathrm{d}z}\frac{\mathrm{d}y}{\mathrm{d}z} & \frac{\mathrm{d}x}{\mathrm{d}z} \end{pmatrix} \begin{pmatrix} \delta_x \\ \delta_y \\ \delta_z \\ \delta_{\phi_x} \\ \delta_{\phi_y} \\ \delta_{\phi_z} \end{pmatrix} , \quad (7)$$

where (x, y) represents the coordinates of the track intersection with the chamber and $(\frac{\mathrm{d}x}{\mathrm{d}z}, \frac{\mathrm{d}y}{\mathrm{d}z})$ the entrance angle. The above matrix is an extension of Eq. (17) in Ref. [10] to include angular residuals $\Delta\frac{\mathrm{d}x}{\mathrm{d}z}$ and $\Delta\frac{\mathrm{d}y}{\mathrm{d}z}$, significantly increasing sensitivity to δ_{ϕ_y} and δ_{ϕ_x}, respectively.

A Voigt distribution, or convolution of a Gaussian with a Cauchy-Lorentzian, is used to model the Gaussian core with large tails. The function

$$f(t;\, t_0,\, \sigma,\, \Gamma) = \int_{-\infty}^{\infty} \frac{1}{\pi} \frac{\Gamma/2}{(t-s-t_0)^2 + (\Gamma/2)^2} \times \frac{1}{\sqrt{2\pi}\sigma} \exp\left(\frac{-s^2}{2\sigma^2}\right) ds \quad , \tag{8}$$

has one variable t with three parameters t_0, σ, and Γ. Close to the peak, the distribution is approximately Gaussian (because $\Gamma \ll \sigma$, typically by a factor of 10), and far from the peak, the distribution is approximately $1/t^2$.

The fit function for the four-dimensional residuals distribution is built from a product of four Voigt distributions. To account for correlations between Δx and $\Delta\frac{\mathrm{d}x}{\mathrm{d}z}$, and between Δy and $\Delta\frac{\mathrm{d}y}{\mathrm{d}z}$, parameters $\alpha_{\Delta x}$ and $\alpha_{\Delta y}$ express linear dependences between them in the fit function, and are allowed to float freely in the alignment fit. The correlation is simply due to the fact that an error in the track direction $\Delta\frac{\mathrm{d}x}{\mathrm{d}z}$ introduced at a distance L upstream of the chamber causes a $\Delta x \approx L\Delta\frac{\mathrm{d}x}{\mathrm{d}z}$ error in position.

Without explicitly substituting the alignment parameters, the full fit function is

$$\begin{aligned} F\Bigg(&\Delta x, \Delta y, \Delta\tfrac{\mathrm{d}x}{\mathrm{d}z}, \Delta\tfrac{\mathrm{d}y}{\mathrm{d}z};\\ &\Delta x_0, \Delta y_0, \Delta\frac{\mathrm{d}x}{\mathrm{d}z}_0, \Delta\frac{\mathrm{d}y}{\mathrm{d}z}_0, \sigma_{\Delta x}, \sigma_{\Delta y}, \sigma_{\Delta\frac{\mathrm{d}x}{\mathrm{d}z}}, \sigma_{\Delta\frac{\mathrm{d}y}{\mathrm{d}z}}, \Gamma_{\Delta x}, \Gamma_{\Delta y}, \Gamma_{\Delta\frac{\mathrm{d}x}{\mathrm{d}z}}, \Gamma_{\Delta\frac{\mathrm{d}y}{\mathrm{d}z}}, \alpha_{\Delta x}, \alpha_{\Delta y}) = \\ &f\left(\Delta x;\, (\Delta x_0 + \alpha_{\Delta x}\Delta\tfrac{\mathrm{d}x}{\mathrm{d}z}),\, \sigma_{\Delta x},\, \Gamma_{\Delta x}\right) \times f\left(\Delta\tfrac{\mathrm{d}x}{\mathrm{d}z};\, \Delta\tfrac{\mathrm{d}x}{\mathrm{d}z}_0,\, \sigma_{\Delta\frac{\mathrm{d}x}{\mathrm{d}z}},\, \Gamma_{\Delta\frac{\mathrm{d}x}{\mathrm{d}z}}\right)\\ &f\left(\Delta y;\, (\Delta y_0 + \alpha_{\Delta y}\Delta\tfrac{\mathrm{d}y}{\mathrm{d}z}),\, \sigma_{\Delta y},\, \Gamma_{\Delta y}\right) \times f\left(\Delta\tfrac{\mathrm{d}y}{\mathrm{d}z};\, \Delta\tfrac{\mathrm{d}y}{\mathrm{d}z}_0,\, \sigma_{\Delta\frac{\mathrm{d}y}{\mathrm{d}z}},\, \Gamma_{\Delta\frac{\mathrm{d}y}{\mathrm{d}z}}\right) \quad . \end{aligned} \tag{9}$$

Substituting Δx_0, Δy_0, $\Delta\frac{\mathrm{d}x}{\mathrm{d}z}_0$, $\Delta\frac{\mathrm{d}y}{\mathrm{d}z}_0$ from Eq. (7) introduces the track position and entrance angle as four new variables and the alignment parameters as six new parameters. All parameter values and estimates of their uncertainties are evaluated by MINUIT, seeded by the truncated mean and RMS of each distribution. An example fit is shown in Fig. 6.

The alignment fit is weighted to reduce the influence of poorly formed segments. The quality of a segment is quantified by χ^2/ndf, rather than uncertainties in its parameters, so segments in the alignment fit are weighted by $w_i = (\mathrm{ndf}/\chi^2)_i / \sum_{i'}(\mathrm{ndf}/\chi^2)_{i'}$ of the segment fits. The objective function minimized by the alignment is $\chi^2 = \sum_i w_i \log F_i$ where F_i is given by Eq. (9) for each segment i. To avoid domination of the fit by a few of the most linear segments, which are not necessarily from the best-determined tracks (unscattered muons), segments with the largest 1% of weights have been excluded.

To resolve unmodeled non-linearities in the residuals, the procedure is applied twice, taking the output of the first iteration as an initial geometry for the second. No subsequent improvements are observed in a third iteration or beyond.

5.1.3 Configuration for Alignment with Cosmic-Ray Muons

The vertical distribution of cosmic rays underground imposed geometric restrictions on the set of chambers that could be aligned with this algorithm. Only barrel wheels -1, 0, $+1$, excluding horizontal sectors 1 and 7 (see Fig. 2), recorded a sufficient number of muons that also crossed the barrel of the tracker to perform an alignment. In addition, the fits for four nearly horizontal

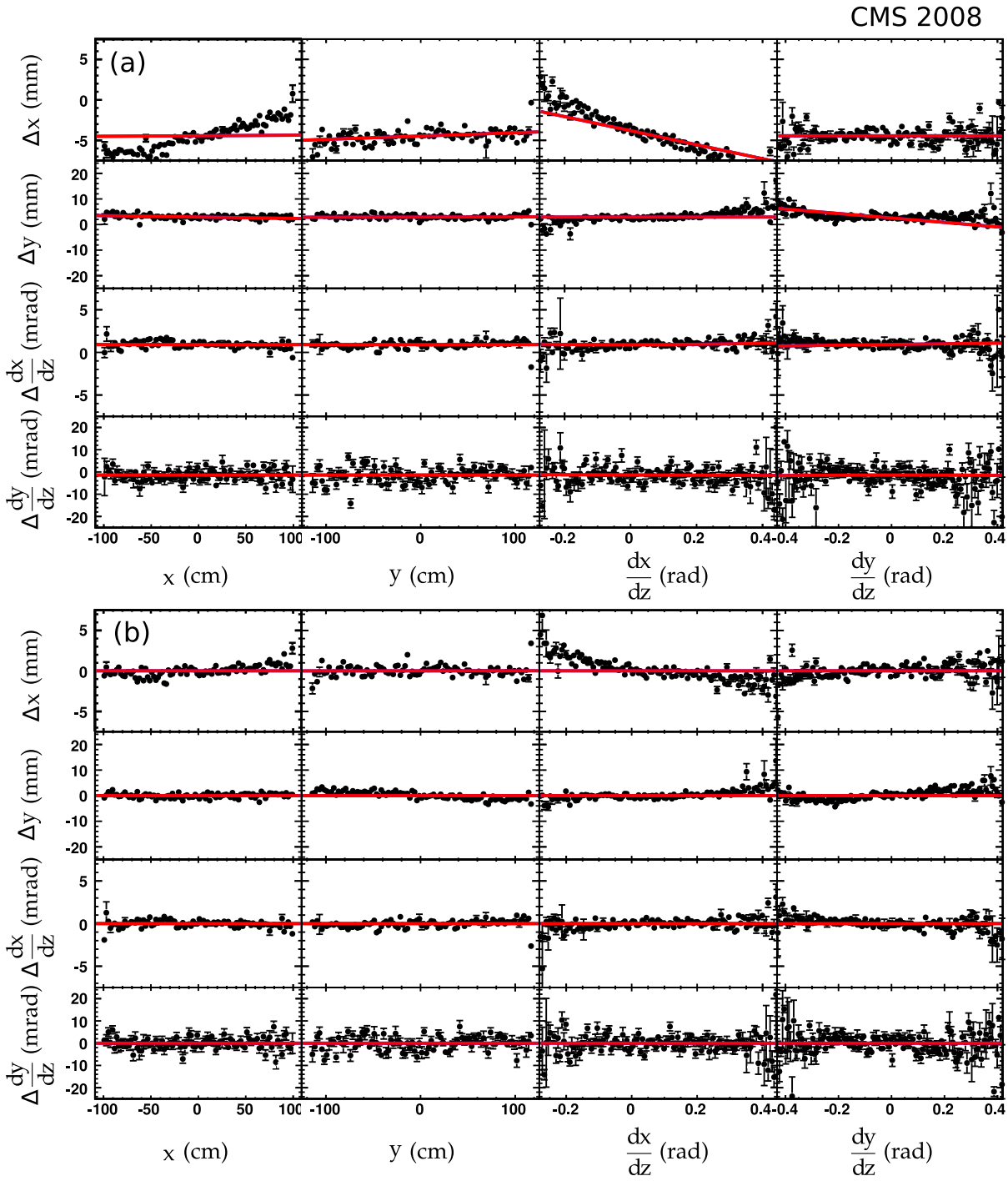

Figure 6: Mean residuals with statistical error bars versus position (x, y) and entrance angle ($\frac{dx}{dz}$, $\frac{dy}{dz}$) in one chamber (DT wheel 0, station 1, sector 10) from cosmic-ray data, (a) before alignment and (b) after alignment. Each bin selects a narrow range of the position or entrance angle component under consideration, but averages over all other variables. The fit function, evaluated at zero in all other variables, is overlaid as lines before and after alignment. Asymmetries in the position and entrance angle distributions allow for misalignments to be manifested in more ways in the averaged residuals than in the projections of the best-fit function, but the fit properly removes these misalignments, resulting in nearly flat lines in all variables.

chambers (in wheel, station, sector (−1, 2, 8), (+1, 3, 8), (−1, 1, 12), and (+1, 2, 2)) failed to converge, all for reasons related to the scarcity of horizontal cosmic ray muons.

For most chambers within the restricted set, however, cosmic-ray muons are sufficiently abundant that the measurement is not statistics-limited. It is therefore possible to apply a tight set of track quality requirements, to control systematic errors:

- $100 < p_T < 200$ GeV/c (nearly straight tracks; the upper limit guarantees statistical independence from one of the cross-checks);
- 12 out of 12 hits in DT chambers of stations 1–3, 8 out of 8 hits in DT chambers of station 4;
- at least 15 hits on the tracker track, with $\chi^2/\mathrm{ndf} < 10$.

The cosmic-ray period included several on-off cycles of the magnetic field, and the full field (3.8 T) periods were shown to result in reproducible alignment parameters with the hardware system [3] and track residuals. Only datasets marked as acceptable for physics with full field from the CMS "run registry" [4] were used. Of the 270 million cosmic-ray triggered events in CRAFT, the above requirements select 100 000 tracks (the reduction is primarily due the p_T selection and the requirement that cosmic-ray trajectories to pass through the tracker), yet statistical uncertainties are typically only 120 μm in δ_x. Systematic errors, which may amount to several hundred microns, dominate the alignment parameter uncertainties, and hence it is better to select the highest-quality muons.

DT chambers in stations 1–3 are aligned in all six degrees of freedom, but chambers of station 4 are only aligned in δ_x, δ_{ϕ_y}, and δ_{ϕ_z}, as these are the most sensitive alignment parameters without Δy and $\Delta\frac{\mathrm{d}y}{\mathrm{d}z}$ residuals (recall that station 4 chambers have no y-measuring superlayer). Unaligned coordinates are not allowed to float in the minimization.

5.2 Monte Carlo Study

To test the alignment algorithm, a large sample of cosmic rays was simulated (using CMSCGEN, described in Ref. [16]), tracks were reconstructed with misaligned muon chambers (2 mm Gaussian smearing in x, 4 mm in y and z, 2 mrad in ϕ_x, ϕ_y, and ϕ_z), and the algorithm was applied to restore the original alignment parameters using only the tracks. To focus on the accuracy of the algorithm itself, the tracker geometry, internal muon layer geometry, magnetic field map, and material distribution were modeled without errors (identical in simulation and reconstruction). All other detector effects were realistically modeled.

The test was performed twice, the first time with 350 000 tracks passing all selection requirements and again with 100 000 tracks (a subsample). The first can be considered an infinite-statistics limit, as statistical uncertainties from MINUIT are typically 3–4 times smaller than the aligned position errors (see Tables 1 and 2). The second matches the statistical precision of CRAFT. Distributions of chamber position errors are presented in Fig. 7.

5.3 Alignment Results: Residuals Distribution

After applying the algorithm to the CRAFT cosmic-ray dataset, the four-component distribution of residuals is found to be centered on zero to the same degree as in the Monte Carlo simulation. Figure 8 presents the residuals distribution of all aligned chambers, where the alignment makes the distribution narrower and smoother. The size of the dataset is also large enough to see the non-Gaussian tails in detail, and that the simulated residuals distribution closely matches the real one. However, the raw residuals do not provide a sensitive probe

Table 1: Statistical uncertainties in simulation and data: uncertainties for all chambers $i = 1$ to N are summarized by presenting $\sqrt{\frac{1}{N}\sum_i \sigma_i^2}$ where σ_i is the statistical uncertainty in one of the six alignment parameters below.

sample	δ_x (mm)	δ_y (mm)	δ_z (mm)	δ_{ϕ_x} (mrad)	δ_{ϕ_y} (mrad)	δ_{ϕ_z} (mrad)
350 k simulation	0.059	0.118	0.248	0.170	0.038	0.072
100 k simulation	0.106	0.210	0.443	0.305	0.069	0.129
100 k data	0.117	0.243	0.512	0.326	0.074	0.146

Table 2: RMS of differences between aligned and true positions of chambers in Monte Carlo simulations (distributions in Fig. 7).

sample	δ_x (mm)	δ_y (mm)	δ_z (mm)	δ_{ϕ_x} (mrad)	δ_{ϕ_y} (mrad)	δ_{ϕ_z} (mrad)
350 k simulation	0.192	0.841	0.630	0.417	0.095	0.287
100 k simulation	0.209	0.889	0.836	0.497	0.148	0.303

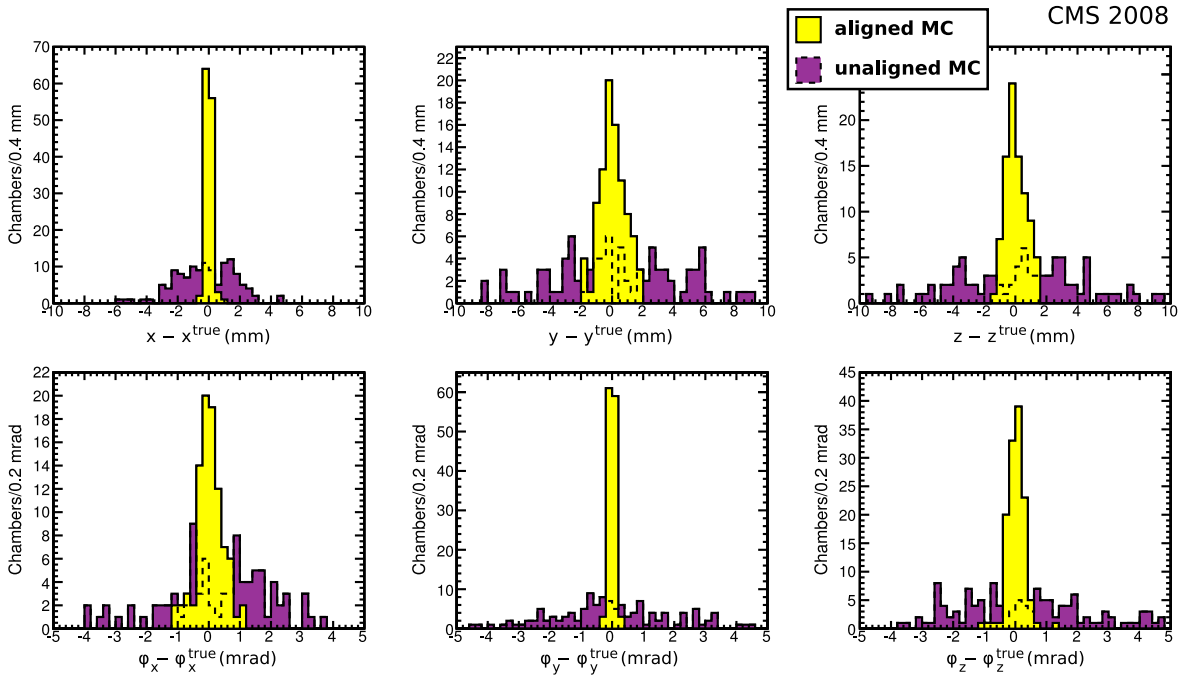

Figure 7: Differences between reconstructed and true positions of muon chambers from an alignment performed with 350 000 simulated cosmic-ray tracks passing selection requirements (only showing chambers in wheels -1, 0, $+1$, all sectors except 1 and 7).

of the alignment accuracy, because alignment corrections are typically much smaller than the width of the distribution.

For a higher sensitivity, the median of the residuals distribution of each chamber is calculated separately, then plotted as a distribution in Fig. 9, with the RMS of the distribution presented in Table 3. The median is less affected by non-Gaussian tails than the mean, and it is a different way of achieving this insensitivity than the Voigt fits used by the algorithm.

5.4 Alignment Results: Cross-check

The analysis of residuals in the previous subsection provides confidence that the alignment algorithm is operating as designed. This section presents a test of the aligned geometry using a significantly different method, namely local segment fits.

A study of alignment parameter consistency for neighboring chambers using overlapping segments from CSCs, as described in Section 4, would provide an ideal cross-check. However, most cosmic rays fall on the barrel, in which chambers do not overlap one another (with the exception of several chambers in station 4). The local alignment quality is therefore checked by comparing local segments from DT chambers in neighboring stations, propagated through only one layer of steel to the next station.

For each sector in a pair of neighboring stations (MB1→MB2, MB2→MB3, and MB3→MB4), segments are linearly propagated from the inner chamber to the outer chamber and the parameters x^{local}, $\frac{\mathrm{d}x}{\mathrm{d}z}^{\text{local}}$ of the propagated segment are compared with those of the segment in the outer chamber, yielding two residuals, Δx^{local}, $\Delta\frac{\mathrm{d}x}{\mathrm{d}z}^{\text{local}}$.

Curvature from the magnetic field is not included in this propagation, but the error is corrected by taking advantage of the fact that contributions to Δx^{local} and $\Delta\frac{\mathrm{d}x}{\mathrm{d}z}^{\text{local}}$ from the magnetic field are charge-dependent. Segments are associated with the corresponding tracker tracks to identify their charge and to select high transverse momentum ($p_T > 50$ GeV/c). Residuals from positively charged muons and negatively charged muons are collected separately, fitted to Gaussian distributions to identify the peaks, and averaged without weights. Since the momentum spectra of positively and negatively charged cosmic-ray muons are the same at this momentum scale, the magnetic field contributions to average Δx^{local} and $\Delta\frac{\mathrm{d}x}{\mathrm{d}z}^{\text{local}}$ cancel, leaving only differences from misalignments. This is the same procedure as used to test sensitivity to the magnetic field by the reference-target algorithm.

Figure 10 shows the results of these averages for each sector and pair of stations, before and after alignment, and Table 4 presents the RMS of each of the presented distributions. The distributions are convolutions of errors in the alignment and errors in the segment-matching. These results therefore only set an upper limit on the systematic uncertainties of the alignment itself. In addition, global distortions of the combined tracker and muon system are not quantified by this method. This results in an upper limit of 0.7 mm in δ_x (proportional to Δx) and 0.6 mrad in δ_{ϕ_y} (approximately proportional to $\Delta\frac{\mathrm{d}x}{\mathrm{d}z}$) for chambers in stations 1–3, and 1.0 mm, 0.7 mrad in station 4.

The uncertainty in point resolution along the line of sight of tracks is therefore bounded between the Monte Carlo prediction (Table 2), which includes only known propagation and detector effects, and this diagnostic, which has its own systematic uncertainties. For stations 1–3, the uncertainty is at best 200 and at worst 700 μm in δ_x.

Muons from proton collisions, which illuminate the endcaps, will enable a local cross-check

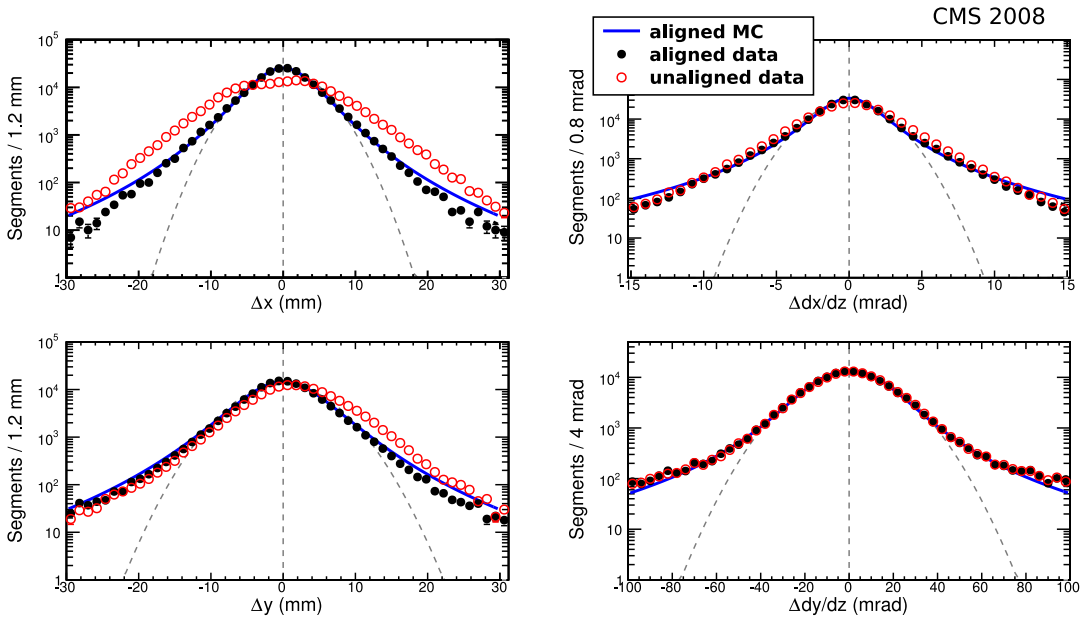

Figure 8: Residuals distributions before and after alignment using CRAFT data. The full curves describe the aligned Monte Carlo prediction and the light dashed curves indicate the peak of each aligned distribution and its Gaussian approximation.

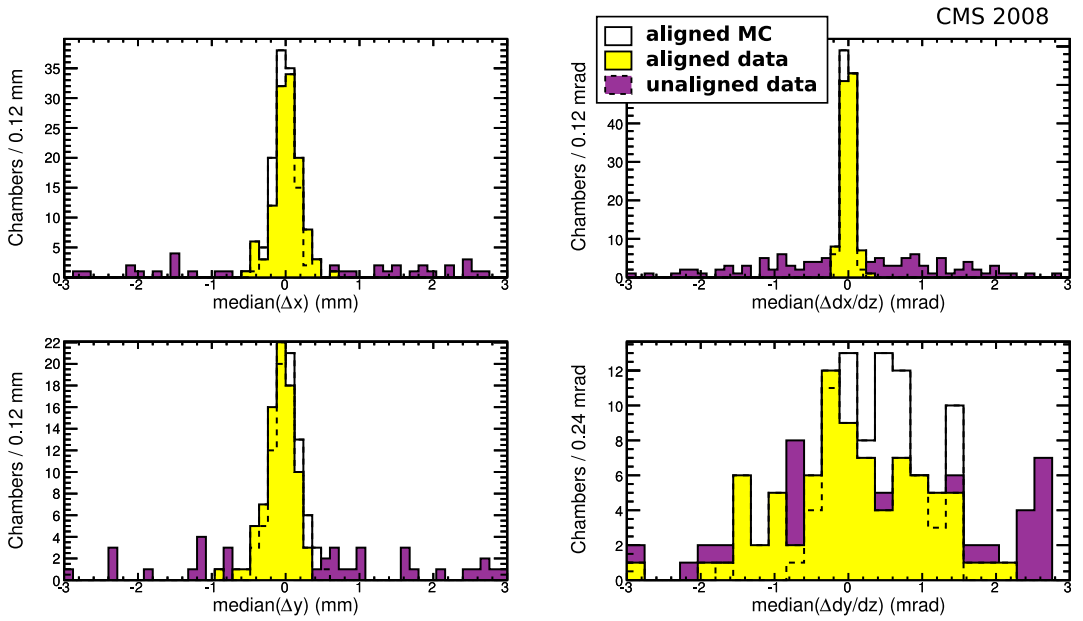

Figure 9: Medians of residuals distributions by chamber (one histogram entry per chamber).

Table 3: RMS of medians of residuals distributions by chamber (distributions in Fig. 9).

	x (mm)	y (mm)	$\frac{dx}{dz}$ (mrad)	$\frac{dy}{dz}$ (mrad)
Aligned MC (100 k)	0.159	0.172	0.066	0.630
Aligned data (100 k)	0.190	0.166	0.085	0.885
Unaligned data (100 k)	5.667	2.570	1.316	1.605

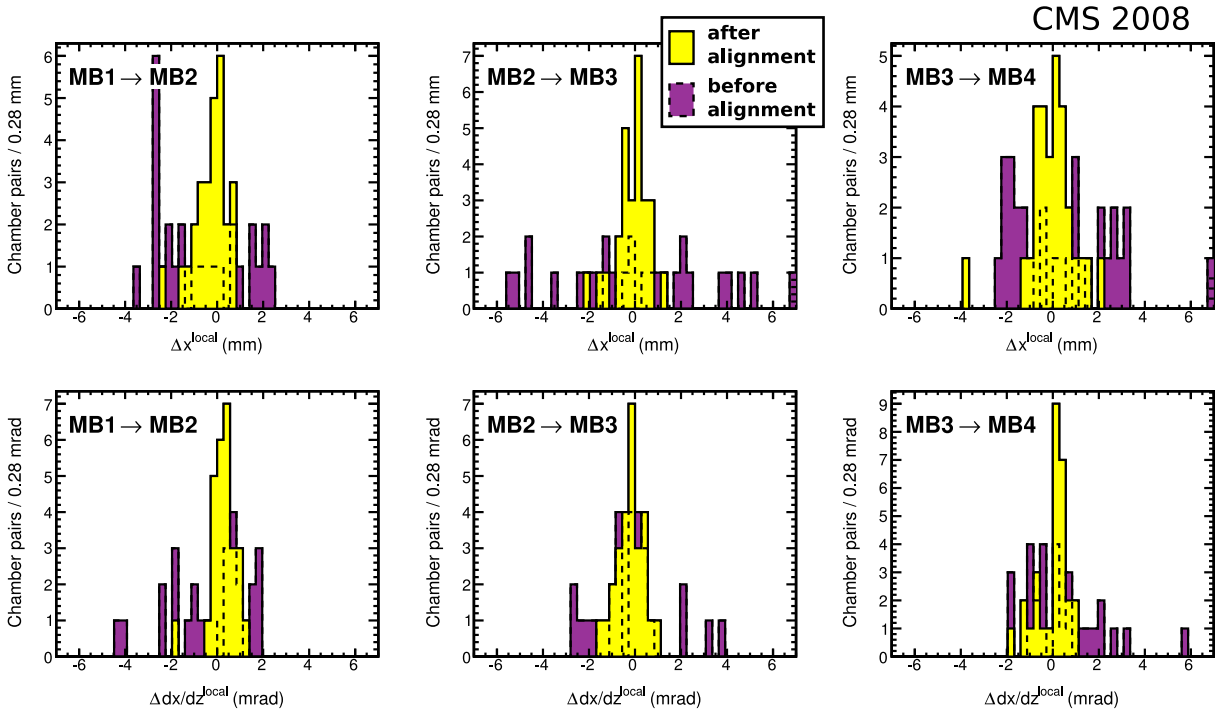

Figure 10: Differences in DT chamber positions and angles between pairs of stations as measured by locally propagated segments. Dark/dashed histograms are before alignment; light histograms are after alignment.

Table 4: RMS of pairwise position and angle differences by station (distributions in Fig. 10).

		Unaligned	Aligned
MB1 → MB2	Δx^{local} (mm)	1.82	0.68
MB1 → MB2	$\Delta \frac{\mathrm{d}x}{\mathrm{d}z}^{\text{local}}$ (mrad)	1.68	0.57
MB2 → MB3	Δx^{local} (mm)	3.20	0.69
MB2 → MB3	$\Delta \frac{\mathrm{d}x}{\mathrm{d}z}^{\text{local}}$ (mrad)	1.56	0.60
MB3 → MB4	Δx^{local} (mm)	2.17	1.06
MB3 → MB4	$\Delta \frac{\mathrm{d}x}{\mathrm{d}z}^{\text{local}}$ (mrad)	1.65	0.70

with the CSC ring method of Section 4. Since the latter has a demonstrated position uncertainty of 270 μm, such a comparison will considerably tighten the bound on alignment resolution uncertainty.

5.5 Alignment Results: Effect on Momentum Measurement

The motivation for the alignment effort is to correct reconstructed muon momentum distributions, so the trajectories of cosmic-ray muons are re-fitted with the new geometry to verify that the resolution has improved. For sensitivity to the effect of misalignments in the muon system, energetic cosmic rays are selected with $p_T > 200$ GeV/c, a sample which is independent of the $100 < p_T < 200$ GeV/c tracks used to perform the alignment. Tracks are reconstructed using hits from the tracker and the first muon station, a simple way to optimize high-momentum muon resolution by increasing the effective lever arm of sagitta measurements while minimizing bias from radiative muon showers, which become prominent at several hundred GeV/c. It also focuses on the connection between the tracker and the first muon station, a pair that was not tested with the segments described in Section 5.4.

The top half and bottom half of the cosmic ray trajectory are reconstructed separately, split at the point of closest approach to the LHC beamline. Any difference in track parameters between the top and bottom fits is purely instrumental: in Fig. 11 the fractional difference in curvature $(\Delta\kappa/(\sqrt{2}\kappa) = (\kappa_{\text{top}} - \kappa_{\text{bottom}})/(\sqrt{2}\kappa)$ where $\kappa = q/p_T$) is plotted before and after alignment; the tracker-only reconstruction is also given, for reference. Assuming that the measurements in the top and bottom parts of CMS are statistically independent with equal resolutions, this plot represents the fractional error in the curvature of tracks, which is approximately equal to the fractional error in its reciprocal, p_T. Some global distortions correlate misalignments in the top and bottom parts of the detector; this test is insensitive to such modes. The fitted resolution is given in Table 5.

The majority of muons in this study have a momentum close to the 200 GeV/c threshold because of the steeply falling distribution of cosmic rays. At 200 GeV/c, the momentum resolution of the combined system is not expected to significantly exceed the resolution of the tracker alone (see Ref. [17], Fig. 1.5), but the biased distribution prior to alignment has been repaired by alignment procedure.

5.6 The Millepede Algorithm

A Millepede algorithm [7] is under development to align the muon chambers relative to the tracker, as an alternative to the reference-target algorithm. Instead of using a general non-linear fitting package to minimize the objective function, Millepede linearizes the problem and solves it with matrix inversion. A potential application of this method is to combine in a single fit measurements from tracker tracks and the locally fitted segments described in Section 5.4, thereby optimizing statistical precision. Before such a generalization is used, however, it must be tuned to reproduce the results of the reference-target algorithm. When configured to use tracker tracks only, the objective function is

$$\chi^2 = \sum_{i}^{\text{chambers}} \sum_{i}^{\text{tracks}} \left(\Delta\vec{x}_j - A_j \cdot \vec{\delta}_i\right)^T \left(\sigma_{\text{residual}}{}^2\right)^{-1}_{ij} \left(\Delta\vec{x}_j - A_j \cdot \vec{\delta}_i\right) \quad , \tag{10}$$

where $\Delta\vec{x} = (\Delta x, \Delta y, \Delta\frac{\mathrm{d}x}{\mathrm{d}z}, \Delta\frac{\mathrm{d}y}{\mathrm{d}z})$, A_j is the matrix in Eq. (7), and $\left(\sigma_{\text{residual}}{}^2\right)^{-1}_{ij}$ is the inverse of the residuals covariance matrix.

To avoid the influence of non-Gaussian tails, noisy channels, and pattern-recognition errors in the determination of the peak of the residuals distribution, large residuals were excluded,

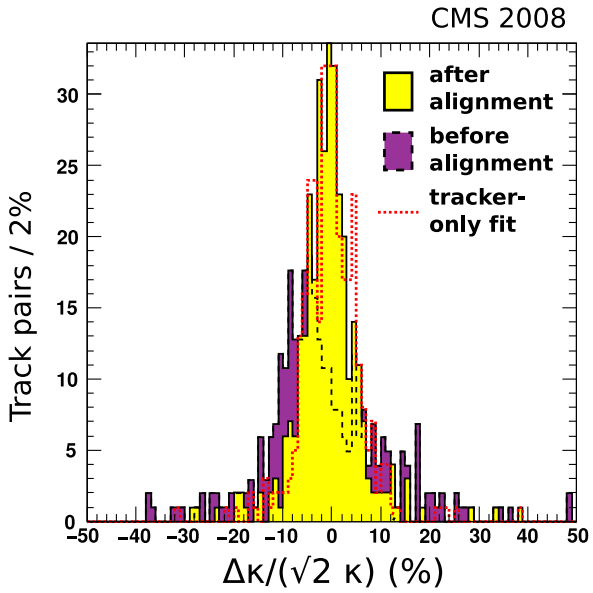

Figure 11: Fractional curvature difference between the top and bottom parts of CMS for muons with $p_T > 200$ GeV/c ($\kappa = q/p_T$). Dark/dashed distribution is before alignment, light is after alignment (using the reference-target algorithm), and the open dotted distribution is tracker-only.

Table 5: RMS and Gaussian core fits of the fractional curvature distributions in Fig. 11. The fits include all data in the central region $\left|\Delta\kappa/(\sqrt{2}\kappa)\right| < 2\times$RMS.

	Gaussian mean (%)	Gaussian width (%)	RMS (%)
Unaligned	-2.5 ± 0.6	8.6 ± 0.5	12.3
Aligned	-0.9 ± 0.3	4.3 ± 0.2	6.9
Tracker-only	0.3 ± 0.3	4.5 ± 0.2	6.4

Table 6: Accuracy of Millepede alignment in Monte Carlo simulations (350 k tracks), varying the selection threshold of the excluded region. The resolution attained with a threshold of $2.5\,\gamma$ reproduces that of the reference-target algorithm presented in Table 2.

selection threshold	δ_x (mm)	δ_y (mm)	δ_z (mm)
$1.0\,\gamma$	0.41	1.05	2.39
$1.5\,\gamma$	0.30	0.89	1.46
$2.0\,\gamma$	0.26	0.84	0.92
$2.5\,\gamma$	0.25	0.84	0.78
$3.0\,\gamma$	0.25	0.85	0.78

symmetrically around the peak, for each of the four residuals components. Threshold values for the excluded region are derived from Cauchy-Lorentzian fits. With x_0 and γ being the mean and half-width at half maximum, only residuals between $x_0 - 2.5\,\gamma$ and $x_0 + 2.5\,\gamma$ enter the sum in Eq. (10) for all four components. The optimum threshold was chosen from the study presented in Table 6, which lists alignment position accuracy as a function of the threshold value.

6 Summary and Discussion

This paper has presented a variety of procedures to align different parts of the muon system with tracks: layers in DT chambers, CSC chambers in rings, and DT chambers in a coordinate frame shared with the tracker. The available data have been fully exploited: horizontal beam-halo and vertical cosmic-ray muons. Through comparisons with independent data, it was shown that the superlayer $r\phi$ resolution is 80 μm within each DT chamber, that the $r\phi$ resolution of CSC chambers is 270 μm within each endcap ring, and that the DT chamber positions along the tracks are known with an accuracy between 200 and 700 μm (stations 1–3, wheels -1, 0, $+1$).

In addition, several new techniques have been introduced. The superlayer structure of DT chambers permits an analysis of layer geometry in a way that uses tracks alone, and therefore rigorously compares the result obtained with tracks with the results from survey measurements. The overlap of CSC rings permits an analytic solution to its alignment. Non-Gaussianity in the physics of track propagation through the steel yoke implies a non-linear extension to the general alignment method.

Techniques which will be useful for re-aligning the muon system with early LHC data have been tested. The favorable distribution of muons from collisions will broaden the applicability of these methods and open new opportunities for cross-checks and diagnostics, which ultimately will lead to a better-understood momentum resolution for high-momentum muons and increased discovery reach for high-energy processes.

Acknowledgements

We thank the technical and administrative staff at CERN and other CMS Institutes, and acknowledge support from: FMSR (Austria); FNRS and FWO (Belgium); CNPq, CAPES, FAPERJ,

and FAPESP (Brazil); MES (Bulgaria); CERN; CAS, MoST, and NSFC (China); COLCIENCIAS (Colombia); MSES (Croatia); RPF (Cyprus); Academy of Sciences and NICPB (Estonia); Academy of Finland, ME, and HIP (Finland); CEA and CNRS/IN2P3 (France); BMBF, DFG, and HGF (Germany); GSRT (Greece); OTKA and NKTH (Hungary); DAE and DST (India); IPM (Iran); SFI (Ireland); INFN (Italy); NRF (Korea); LAS (Lithuania); CINVESTAV, CONACYT, SEP, and UASLP-FAI (Mexico); PAEC (Pakistan); SCSR (Poland); FCT (Portugal); JINR (Armenia, Belarus, Georgia, Ukraine, Uzbekistan); MST and MAE (Russia); MSTDS (Serbia); MICINN and CPAN (Spain); Swiss Funding Agencies (Switzerland); NSC (Taipei); TUBITAK and TAEK (Turkey); STFC (United Kingdom); DOE and NSF (USA). Individuals have received support from the Marie-Curie IEF program (European Union); the Leventis Foundation; the A. P. Sloan Foundation; and the Alexander von Humboldt Foundation.

References

[1] CMS Collaboration, "The CMS experiment at the CERN LHC", *JINST* **3** (2008) S08004. doi:10.1088/1748-0221/3/08/S08004.

[2] L. Evans and P. Bryant, (eds.), "LHC Machine", *JINST* **3** (2008) S08001. doi:10.1088/1748-0221/3/08/S08001.

[3] CMS Collaboration, "Aligning the CMS Muon Chambers with the Muon Alignment System during the Cosmic Run of 2008", *submitted to JINST* (2009).

[4] CMS Collaboration, "Commissioning of the CMS Experiment and the Cosmic Run at Four Tesla", *submitted to JINST* (2009).

[5] CMS Collaboration, "From Detector to Analysis: CMS Data Processing Workflows During an Extended Cosmic Ray Run", *submitted to JINST* (2009).

[6] CMS Collaboration, "Performance of the CMS Cathode Strip Chambers with Cosmic Rays", *submitted to JINST* (2009).

[7] V. Blobel, "Software alignment for tracking detectors", *Nucl. Instrum. Meth.* **A566** (2006) 5–13. doi:10.1016/j.nima.2006.05.157.

[8] V. Drollinger, "Simulation of Beam Halo and Cosmic Muons", *CMS Note* **2005/012** (2005). http://cms-secr.web.cern.ch/cms-secr/documents/05/note05_012.pdf.

[9] R. Goudard, J. F. Fuchs, and J. D. Maillefaud, "Photogrammetry of the YE−2 Face Z− ME−3 Layer CERN SX5". https://edms.cern.ch/document/866869/1.

[10] V. Karimaki, A. Heikkinen, T. Lampen, and T. Linden, "Sensor alignment by tracks", *In the Proceedings of 2003 Conference for Computing in High-Energy and Nuclear Physics (CHEP 03), La Jolla, California, 24-28 Mar 2003, pp TULT008* (2003) arXiv:physics/0306034.

[11] CMS Collaboration, "Alignment of the CMS Silicon Tracker during Commissioning with Cosmic Rays", *submitted to JINST* (2009) arXiv:0910.2505.

[12] F. James and M. Roos, "Minuit: A System for Function Minimization and Analysis of the Parameter Errors and Correlations", *Comput. Phys. Commun.* **10** (1975) 343–367. doi:10.1016/0010-4655(75)90039-9.

[13] CMS Collaboration, "Precise Mapping of the Magnetic Field in the CMS Barrel Yoke using Cosmic Rays", *submitted to JINST* (2009).

[14] G. Flucke, P. Schleper, G. Steinbruck, and M. Stoye, "CMS silicon tracker alignment strategy with the Millepede II algorithm", *JINST* **3** (2008) P09002. doi:10.1088/1748-0221/3/09/P09002.

[15] M. Stoye and P. Schleper (dir.), "Calibration and Alignment of the CMS Silicon Tracking Detector". PhD thesis, Univ. Hamburg, Hamburg, 2007. http://cdsweb.cern.ch/record/1047047.

[16] P. Biallass and T. Hebbeker, "Parametrization of the Cosmic Muon Flux for the Generator CMSCGEN", arXiv:0907.5514.

[17] CMS Collaboration, "CMS technical design report, volume II: Physics performance", *J. Phys.* **G34** (2007) 995–1579. doi:10.1088/0954-3899/34/6/S01.

A The CMS Collaboration

Yerevan Physics Institute, Yerevan, Armenia
S. Chatrchyan, V. Khachatryan, A.M. Sirunyan

Institut für Hochenergiephysik der OeAW, Wien, Austria
W. Adam, B. Arnold, H. Bergauer, T. Bergauer, M. Dragicevic, M. Eichberger, J. Erö, M. Friedl, R. Frühwirth, V.M. Ghete, J. Hammer[1], S. Hänsel, M. Hoch, N. Hörmann, J. Hrubec, M. Jeitler, G. Kasieczka, K. Kastner, M. Krammer, D. Liko, I. Magrans de Abril, I. Mikulec, F. Mittermayr, B. Neuherz, M. Oberegger, M. Padrta, M. Pernicka, H. Rohringer, S. Schmid, R. Schöfbeck, T. Schreiner, R. Stark, H. Steininger, J. Strauss, A. Taurok, F. Teischinger, T. Themel, D. Uhl, P. Wagner, W. Waltenberger, G. Walzel, E. Widl, C.-E. Wulz

National Centre for Particle and High Energy Physics, Minsk, Belarus
V. Chekhovsky, O. Dvornikov, I. Emeliantchik, A. Litomin, V. Makarenko, I. Marfin, V. Mossolov, N. Shumeiko, A. Solin, R. Stefanovitch, J. Suarez Gonzalez, A. Tikhonov

Research Institute for Nuclear Problems, Minsk, Belarus
A. Fedorov, A. Karneyeu, M. Korzhik, V. Panov, R. Zuyeuski

Research Institute of Applied Physical Problems, Minsk, Belarus
P. Kuchinsky

Universiteit Antwerpen, Antwerpen, Belgium
W. Beaumont, L. Benucci, M. Cardaci, E.A. De Wolf, E. Delmeire, D. Druzhkin, M. Hashemi, X. Janssen, T. Maes, L. Mucibello, S. Ochesanu, R. Rougny, M. Selvaggi, H. Van Haevermaet, P. Van Mechelen, N. Van Remortel

Vrije Universiteit Brussel, Brussel, Belgium
V. Adler, S. Beauceron, S. Blyweert, J. D'Hondt, S. De Weirdt, O. Devroede, J. Heyninck, A. Kalogeropoulos, J. Maes, M. Maes, M.U. Mozer, S. Tavernier, W. Van Doninck[1], P. Van Mulders, I. Villella

Université Libre de Bruxelles, Bruxelles, Belgium
O. Bouhali, E.C. Chabert, O. Charaf, B. Clerbaux, G. De Lentdecker, V. Dero, S. Elgammal, A.P.R. Gay, G.H. Hammad, P.E. Marage, S. Rugovac, C. Vander Velde, P. Vanlaer, J. Wickens

Ghent University, Ghent, Belgium
M. Grunewald, B. Klein, A. Marinov, D. Ryckbosch, F. Thyssen, M. Tytgat, L. Vanelderen, P. Verwilligen

Université Catholique de Louvain, Louvain-la-Neuve, Belgium
S. Basegmez, G. Bruno, J. Caudron, C. Delaere, P. Demin, D. Favart, A. Giammanco, G. Grégoire, V. Lemaitre, O. Militaru, S. Ovyn, K. Piotrzkowski[1], L. Quertenmont, N. Schul

Université de Mons, Mons, Belgium
N. Beliy, E. Daubie

Centro Brasileiro de Pesquisas Fisicas, Rio de Janeiro, Brazil
G.A. Alves, M.E. Pol, M.H.G. Souza

Universidade do Estado do Rio de Janeiro, Rio de Janeiro, Brazil
W. Carvalho, D. De Jesus Damiao, C. De Oliveira Martins, S. Fonseca De Souza, L. Mundim, V. Oguri, A. Santoro, S.M. Silva Do Amaral, A. Sznajder

Instituto de Fisica Teorica, Universidade Estadual Paulista, Sao Paulo, Brazil

T.R. Fernandez Perez Tomei, M.A. Ferreira Dias, E. M. Gregores[2], S.F. Novaes

Institute for Nuclear Research and Nuclear Energy, Sofia, Bulgaria
K. Abadjiev[1], T. Anguelov, J. Damgov, N. Darmenov[1], L. Dimitrov, V. Genchev[1], P. Iaydjiev, S. Piperov, S. Stoykova, G. Sultanov, R. Trayanov, I. Vankov

University of Sofia, Sofia, Bulgaria
A. Dimitrov, M. Dyulendarova, V. Kozhuharov, L. Litov, E. Marinova, M. Mateev, B. Pavlov, P. Petkov, Z. Toteva[1]

Institute of High Energy Physics, Beijing, China
G.M. Chen, H.S. Chen, W. Guan, C.H. Jiang, D. Liang, B. Liu, X. Meng, J. Tao, J. Wang, Z. Wang, Z. Xue, Z. Zhang

State Key Lab. of Nucl. Phys. and Tech., Peking University, Beijing, China
Y. Ban, J. Cai, Y. Ge, S. Guo, Z. Hu, Y. Mao, S.J. Qian, H. Teng, B. Zhu

Universidad de Los Andes, Bogota, Colombia
C. Avila, M. Baquero Ruiz, C.A. Carrillo Montoya, A. Gomez, B. Gomez Moreno, A.A. Ocampo Rios, A.F. Osorio Oliveros, D. Reyes Romero, J.C. Sanabria

Technical University of Split, Split, Croatia
N. Godinovic, K. Lelas, R. Plestina, D. Polic, I. Puljak

University of Split, Split, Croatia
Z. Antunovic, M. Dzelalija

Institute Rudjer Boskovic, Zagreb, Croatia
V. Brigljevic, S. Duric, K. Kadija, S. Morovic

University of Cyprus, Nicosia, Cyprus
R. Fereos, M. Galanti, J. Mousa, A. Papadakis, F. Ptochos, P.A. Razis, D. Tsiakkouri, Z. Zinonos

National Institute of Chemical Physics and Biophysics, Tallinn, Estonia
A. Hektor, M. Kadastik, K. Kannike, M. Müntel, M. Raidal, L. Rebane

Helsinki Institute of Physics, Helsinki, Finland
E. Anttila, S. Czellar, J. Härkönen, A. Heikkinen, V. Karimäki, R. Kinnunen, J. Klem, M.J. Kortelainen, T. Lampén, K. Lassila-Perini, S. Lehti, T. Lindén, P. Luukka, T. Mäenpää, J. Nysten, E. Tuominen, J. Tuominiemi, D. Ungaro, L. Wendland

Lappeenranta University of Technology, Lappeenranta, Finland
K. Banzuzi, A. Korpela, T. Tuuva

Laboratoire d'Annecy-le-Vieux de Physique des Particules, IN2P3-CNRS, Annecy-le-Vieux, France
P. Nedelec, D. Sillou

DSM/IRFU, CEA/Saclay, Gif-sur-Yvette, France
M. Besancon, R. Chipaux, M. Dejardin, D. Denegri, J. Descamps, B. Fabbro, J.L. Faure, F. Ferri, S. Ganjour, F.X. Gentit, A. Givernaud, P. Gras, G. Hamel de Monchenault, P. Jarry, M.C. Lemaire, E. Locci, J. Malcles, M. Marionneau, L. Millischer, J. Rander, A. Rosowsky, D. Rousseau, M. Titov, P. Verrecchia

Laboratoire Leprince-Ringuet, Ecole Polytechnique, IN2P3-CNRS, Palaiseau, France
S. Baffioni, L. Bianchini, M. Bluj[3], P. Busson, C. Charlot, L. Dobrzynski, R. Granier de Cassagnac, M. Haguenauer, P. Miné, P. Paganini, Y. Sirois, C. Thiebaux, A. Zabi

Institut Pluridisciplinaire Hubert Curien, Université de Strasbourg, Université de Haute Alsace Mulhouse, CNRS/IN2P3, Strasbourg, France
J.-L. Agram[4], A. Besson, D. Bloch, D. Bodin, J.-M. Brom, E. Conte[4], F. Drouhin[4], J.-C. Fontaine[4], D. Gelé, U. Goerlach, L. Gross, P. Juillot, A.-C. Le Bihan, Y. Patois, J. Speck, P. Van Hove

Université de Lyon, Université Claude Bernard Lyon 1, CNRS-IN2P3, Institut de Physique Nucléaire de Lyon, Villeurbanne, France
C. Baty, M. Bedjidian, J. Blaha, G. Boudoul, H. Brun, N. Chanon, R. Chierici, D. Contardo, P. Depasse, T. Dupasquier, H. El Mamouni, F. Fassi[5], J. Fay, S. Gascon, B. Ille, T. Kurca, T. Le Grand, M. Lethuillier, N. Lumb, L. Mirabito, S. Perries, M. Vander Donckt, P. Verdier

E. Andronikashvili Institute of Physics, Academy of Science, Tbilisi, Georgia
N. Djaoshvili, N. Roinishvili, V. Roinishvili

Institute of High Energy Physics and Informatization, Tbilisi State University, Tbilisi, Georgia
N. Amaglobeli

RWTH Aachen University, I. Physikalisches Institut, Aachen, Germany
R. Adolphi, G. Anagnostou, R. Brauer, W. Braunschweig, M. Edelhoff, H. Esser, L. Feld, W. Karpinski, A. Khomich, K. Klein, N. Mohr, A. Ostaptchouk, D. Pandoulas, G. Pierschel, F. Raupach, S. Schael, A. Schultz von Dratzig, G. Schwering, D. Sprenger, M. Thomas, M. Weber, B. Wittmer, M. Wlochal

RWTH Aachen University, III. Physikalisches Institut A, Aachen, Germany
O. Actis, G. Altenhöfer, W. Bender, P. Biallass, M. Erdmann, G. Fetchenhauer[1], J. Frangenheim, T. Hebbeker, G. Hilgers, A. Hinzmann, K. Hoepfner, C. Hof, M. Kirsch, T. Klimkovich, P. Kreuzer[1], D. Lanske[†], M. Merschmeyer, A. Meyer, B. Philipps, H. Pieta, H. Reithler, S.A. Schmitz, L. Sonnenschein, M. Sowa, J. Steggemann, H. Szczesny, D. Teyssier, C. Zeidler

RWTH Aachen University, III. Physikalisches Institut B, Aachen, Germany
M. Bontenackels, M. Davids, M. Duda, G. Flügge, H. Geenen, M. Giffels, W. Haj Ahmad, T. Hermanns, D. Heydhausen, S. Kalinin, T. Kress, A. Linn, A. Nowack, L. Perchalla, M. Poettgens, O. Pooth, P. Sauerland, A. Stahl, D. Tornier, M.H. Zoeller

Deutsches Elektronen-Synchrotron, Hamburg, Germany
M. Aldaya Martin, U. Behrens, K. Borras, A. Campbell, E. Castro, D. Dammann, G. Eckerlin, A. Flossdorf, G. Flucke, A. Geiser, D. Hatton, J. Hauk, H. Jung, M. Kasemann, I. Katkov, C. Kleinwort, H. Kluge, A. Knutsson, E. Kuznetsova, W. Lange, W. Lohmann, R. Mankel[1], M. Marienfeld, A.B. Meyer, S. Miglioranzi, J. Mnich, M. Ohlerich, J. Olzem, A. Parenti, C. Rosemann, R. Schmidt, T. Schoerner-Sadenius, D. Volyanskyy, C. Wissing, W.D. Zeuner[1]

University of Hamburg, Hamburg, Germany
C. Autermann, F. Bechtel, J. Draeger, D. Eckstein, U. Gebbert, K. Kaschube, G. Kaussen, R. Klanner, B. Mura, S. Naumann-Emme, F. Nowak, U. Pein, C. Sander, P. Schleper, T. Schum, H. Stadie, G. Steinbrück, J. Thomsen, R. Wolf

Institut für Experimentelle Kernphysik, Karlsruhe, Germany
J. Bauer, P. Blüm, V. Buege, A. Cakir, T. Chwalek, W. De Boer, A. Dierlamm, G. Dirkes, M. Feindt, U. Felzmann, M. Frey, A. Furgeri, J. Gruschke, C. Hackstein, F. Hartmann[1], S. Heier, M. Heinrich, H. Held, D. Hirschbuehl, K.H. Hoffmann, S. Honc, C. Jung, T. Kuhr, T. Liamsuwan, D. Martschei, S. Mueller, Th. Müller, M.B. Neuland, M. Niegel, O. Oberst, A. Oehler, J. Ott, T. Peiffer, D. Piparo, G. Quast, K. Rabbertz, F. Ratnikov, N. Ratnikova, M. Renz, C. Saout[1], G. Sartisohn, A. Scheurer, P. Schieferdecker, F.-P. Schilling, G. Schott, H.J. Simonis,

F.M. Stober, P. Sturm, D. Troendle, A. Trunov, W. Wagner, J. Wagner-Kuhr, M. Zeise, V. Zhukov[6], E.B. Ziebarth

Institute of Nuclear Physics "Demokritos", Aghia Paraskevi, Greece
G. Daskalakis, T. Geralis, K. Karafasoulis, A. Kyriakis, D. Loukas, A. Markou, C. Markou, C. Mavrommatis, E. Petrakou, A. Zachariadou

University of Athens, Athens, Greece
L. Gouskos, P. Katsas, A. Panagiotou[1]

University of Ioánnina, Ioánnina, Greece
I. Evangelou, P. Kokkas, N. Manthos, I. Papadopoulos, V. Patras, F.A. Triantis

KFKI Research Institute for Particle and Nuclear Physics, Budapest, Hungary
G. Bencze[1], L. Boldizsar, G. Debreczeni, C. Hajdu[1], S. Hernath, P. Hidas, D. Horvath[7], K. Krajczar, A. Laszlo, G. Patay, F. Sikler, N. Toth, G. Vesztergombi

Institute of Nuclear Research ATOMKI, Debrecen, Hungary
N. Beni, G. Christian, J. Imrek, J. Molnar, D. Novak, J. Palinkas, G. Szekely, Z. Szillasi[1], K. Tokesi, V. Veszpremi

University of Debrecen, Debrecen, Hungary
A. Kapusi, G. Marian, P. Raics, Z. Szabo, Z.L. Trocsanyi, B. Ujvari, G. Zilizi

Panjab University, Chandigarh, India
S. Bansal, H.S. Bawa, S.B. Beri, V. Bhatnagar, M. Jindal, M. Kaur, R. Kaur, J.M. Kohli, M.Z. Mehta, N. Nishu, L.K. Saini, A. Sharma, A. Singh, J.B. Singh, S.P. Singh

University of Delhi, Delhi, India
S. Ahuja, S. Arora, S. Bhattacharya[8], S. Chauhan, B.C. Choudhary, P. Gupta, S. Jain, S. Jain, M. Jha, A. Kumar, K. Ranjan, R.K. Shivpuri, A.K. Srivastava

Bhabha Atomic Research Centre, Mumbai, India
R.K. Choudhury, D. Dutta, S. Kailas, S.K. Kataria, A.K. Mohanty, L.M. Pant, P. Shukla, A. Topkar

Tata Institute of Fundamental Research - EHEP, Mumbai, India
T. Aziz, M. Guchait[9], A. Gurtu, M. Maity[10], D. Majumder, G. Majumder, K. Mazumdar, A. Nayak, A. Saha, K. Sudhakar

Tata Institute of Fundamental Research - HECR, Mumbai, India
S. Banerjee, S. Dugad, N.K. Mondal

Institute for Studies in Theoretical Physics & Mathematics (IPM), Tehran, Iran
H. Arfaei, H. Bakhshiansohi, A. Fahim, A. Jafari, M. Mohammadi Najafabadi, A. Moshaii, S. Paktinat Mehdiabadi, S. Rouhani, B. Safarzadeh, M. Zeinali

University College Dublin, Dublin, Ireland
M. Felcini

INFN Sezione di Bari [a], Università di Bari [b], Politecnico di Bari [c], Bari, Italy
M. Abbrescia[a,b], L. Barbone[a], F. Chiumarulo[a], A. Clemente[a], A. Colaleo[a], D. Creanza[a,c], G. Cuscela[a], N. De Filippis[a], M. De Palma[a,b], G. De Robertis[a], G. Donvito[a], F. Fedele[a], L. Fiore[a], M. Franco[a], G. Iaselli[a,c], N. Lacalamita[a], F. Loddo[a], L. Lusito[a,b], G. Maggi[a,c], M. Maggi[a], N. Manna[a,b], B. Marangelli[a,b], S. My[a,c], S. Natali[a,b], S. Nuzzo[a,b], G. Papagni[a], S. Piccolomo[a], G.A. Pierro[a], C. Pinto[a], A. Pompili[a,b], G. Pugliese[a,c], R. Rajan[a], A. Ranieri[a], F. Romano[a,c],

G. Roselli[a,b], G. Selvaggi[a,b], Y. Shinde[a], L. Silvestris[a], S. Tupputi[a,b], G. Zito[a]

INFN Sezione di Bologna [a], Universita di Bologna [b], Bologna, Italy
G. Abbiendi[a], W. Bacchi[a,b], A.C. Benvenuti[a], M. Boldini[a], D. Bonacorsi[a], S. Braibant-Giacomelli[a,b], V.D. Cafaro[a], S.S. Caiazza[a], P. Capiluppi[a,b], A. Castro[a,b], F.R. Cavallo[a], G. Codispoti[a,b], M. Cuffiani[a,b], I. D'Antone[a], G.M. Dallavalle[a,1], F. Fabbri[a], A. Fanfani[a,b], D. Fasanella[a], P. Giacomelli[a], V. Giordano[a], M. Giunta[a,1], C. Grandi[a], M. Guerzoni[a], S. Marcellini[a], G. Masetti[a,b], A. Montanari[a], F.L. Navarria[a,b], F. Odorici[a], G. Pellegrini[a], A. Perrotta[a], A.M. Rossi[a,b], T. Rovelli[a,b], G. Siroli[a,b], G. Torromeo[a], R. Travaglini[a,b]

INFN Sezione di Catania [a], Universita di Catania [b], Catania, Italy
S. Albergo[a,b], S. Costa[a,b], R. Potenza[a,b], A. Tricomi[a,b], C. Tuve[a]

INFN Sezione di Firenze [a], Universita di Firenze [b], Firenze, Italy
G. Barbagli[a], G. Broccolo[a,b], V. Ciulli[a,b], C. Civinini[a], R. D'Alessandro[a,b], E. Focardi[a,b], S. Frosali[a,b], E. Gallo[a], C. Genta[a,b], G. Landi[a,b], P. Lenzi[a,b,1], M. Meschini[a], S. Paoletti[a], G. Sguazzoni[a], A. Tropiano[a]

INFN Laboratori Nazionali di Frascati, Frascati, Italy
L. Benussi, M. Bertani, S. Bianco, S. Colafranceschi[11], D. Colonna[11], F. Fabbri, M. Giardoni, L. Passamonti, D. Piccolo, D. Pierluigi, B. Ponzio, A. Russo

INFN Sezione di Genova, Genova, Italy
P. Fabbricatore, R. Musenich

INFN Sezione di Milano-Biccoca [a], Universita di Milano-Bicocca [b], Milano, Italy
A. Benaglia[a], M. Calloni[a], G.B. Cerati[a,b,1], P. D'Angelo[a], F. De Guio[a], F.M. Farina[a], A. Ghezzi[a], P. Govoni[a,b], M. Malberti[a,b,1], S. Malvezzi[a], A. Martelli[a], D. Menasce[a], V. Miccio[a,b], L. Moroni[a], P. Negri[a,b], M. Paganoni[a,b], D. Pedrini[a], A. Pullia[a,b], S. Ragazzi[a,b], N. Redaelli[a], S. Sala[a], R. Salerno[a,b], T. Tabarelli de Fatis[a,b], V. Tancini[a,b], S. Taroni[a,b]

INFN Sezione di Napoli [a], Universita di Napoli "Federico II" [b], Napoli, Italy
S. Buontempo[a], N. Cavallo[a], A. Cimmino[a,b,1], M. De Gruttola[a,b,1], F. Fabozzi[a,12], A.O.M. Iorio[a], L. Lista[a], D. Lomidze[a], P. Noli[a,b], P. Paolucci[a], C. Sciacca[a,b]

INFN Sezione di Padova [a], Università di Padova [b], Padova, Italy
P. Azzi[a,1], N. Bacchetta[a], L. Barcellan[a], P. Bellan[a,b,1], M. Bellato[a], M. Benettoni[a], M. Biasotto[a,13], D. Bisello[a,b], E. Borsato[a,b], A. Branca[a], R. Carlin[a,b], L. Castellani[a], P. Checchia[a], E. Conti[a], F. Dal Corso[a], M. De Mattia[a,b], T. Dorigo[a], U. Dosselli[a], F. Fanzago[a], F. Gasparini[a,b], U. Gasparini[a,b], P. Giubilato[a,b], F. Gonella[a], A. Gresele[a,14], M. Gulmini[a,13], A. Kaminskiy[a,b], S. Lacaprara[a,13], I. Lazzizzera[a,14], M. Margoni[a,b], G. Maron[a,13], S. Mattiazzo[a,b], M. Mazzucato[a], M. Meneghelli[a], A.T. Meneguzzo[a,b], M. Michelotto[a], F. Montecassiano[a], M. Nespolo[a], M. Passaseo[a], M. Pegoraro[a], L. Perrozzi[a], N. Pozzobon[a,b], P. Ronchese[a,b], F. Simonetto[a,b], N. Toniolo[a], E. Torassa[a], M. Tosi[a,b], A. Triossi[a], S. Vanini[a,b], S. Ventura[a], P. Zotto[a,b], G. Zumerle[a,b]

INFN Sezione di Pavia [a], Universita di Pavia [b], Pavia, Italy
P. Baesso[a,b], U. Berzano[a], S. Bricola[a], M.M. Necchi[a,b], D. Pagano[a,b], S.P. Ratti[a,b], C. Riccardi[a,b], P. Torre[a,b], A. Vicini[a], P. Vitulo[a,b], C. Viviani[a,b]

INFN Sezione di Perugia [a], Universita di Perugia [b], Perugia, Italy
D. Aisa[a], S. Aisa[a], E. Babucci[a], M. Biasini[a,b], G.M. Bilei[a], B. Caponeri[a,b], B. Checcucci[a], N. Dinu[a], L. Fanò[a], L. Farnesini[a], P. Lariccia[a,b], A. Lucaroni[a,b], G. Mantovani[a,b], A. Nappi[a,b], A. Piluso[a], V. Postolache[a], A. Santocchia[a,b], L. Servoli[a], D. Tonoiu[a], A. Vedaee[a], R. Volpe[a,b]

INFN Sezione di Pisa [a], Universita di Pisa [b], Scuola Normale Superiore di Pisa [c], Pisa, Italy
P. Azzurri[a,c], G. Bagliesi[a], J. Bernardini[a,b], L. Berretta[a], T. Boccali[a], A. Bocci[a,c], L. Borrello[a,c], F. Bosi[a], F. Calzolari[a], R. Castaldi[a], R. Dell'Orso[a], F. Fiori[a,b], L. Foà[a,c], S. Gennai[a,c], A. Giassi[a], A. Kraan[a], F. Ligabue[a,c], T. Lomtadze[a], F. Mariani[a], L. Martini[a], M. Massa[a], A. Messineo[a,b], A. Moggi[a], F. Palla[a], F. Palmonari[a], G. Petragnani[a], G. Petrucciani[a,c], F. Raffaelli[a], S. Sarkar[a], G. Segneri[a], A.T. Serban[a], P. Spagnolo[a,1], R. Tenchini[a,1], S. Tolaini[a], G. Tonelli[a,b,1], A. Venturi[a], P.G. Verdini[a]

INFN Sezione di Roma [a], Universita di Roma "La Sapienza" [b], Roma, Italy
S. Baccaro[a,15], L. Barone[a,b], A. Bartoloni[a], F. Cavallari[a,1], I. Dafinei[a], D. Del Re[a,b], E. Di Marco[a,b], M. Diemoz[a], D. Franci[a,b], E. Longo[a,b], G. Organtini[a,b], A. Palma[a,b], F. Pandolfi[a,b], R. Paramatti[a,1], F. Pellegrino[a], S. Rahatlou[a,b], C. Rovelli[a]

INFN Sezione di Torino [a], Università di Torino [b], Università del Piemonte Orientale (Novara) [c], Torino, Italy
G. Alampi[a], N. Amapane[a,b], R. Arcidiacono[a,b], S. Argiro[a,b], M. Arneodo[a,c], C. Biino[a], M.A. Borgia[a,b], C. Botta[a,b], N. Cartiglia[a], R. Castello[a,b], G. Cerminara[a,b], M. Costa[a,b], D. Dattola[a], G. Dellacasa[a], N. Demaria[a], G. Dughera[a], F. Dumitrache[a], A. Graziano[a,b], C. Mariotti[a], M. Marone[a,b], S. Maselli[a], E. Migliore[a,b], G. Mila[a,b], V. Monaco[a,b], M. Musich[a,b], M. Nervo[a,b], M.M. Obertino[a,c], S. Oggero[a,b], R. Panero[a], N. Pastrone[a], M. Pelliccioni[a,b], A. Romero[a,b], M. Ruspa[a,c], R. Sacchi[a,b], A. Solano[a,b], A. Staiano[a], P.P. Trapani[a,b,1], D. Trocino[a,b], A. Vilela Pereira[a,b], L. Visca[a,b], A. Zampieri[a]

INFN Sezione di Trieste [a], Universita di Trieste [b], Trieste, Italy
F. Ambroglini[a,b], S. Belforte[a], F. Cossutti[a], G. Della Ricca[a,b], B. Gobbo[a], A. Penzo[a]

Kyungpook National University, Daegu, Korea
S. Chang, J. Chung, D.H. Kim, G.N. Kim, D.J. Kong, H. Park, D.C. Son

Wonkwang University, Iksan, Korea
S.Y. Bahk

Chonnam National University, Kwangju, Korea
S. Song

Konkuk University, Seoul, Korea
S.Y. Jung

Korea University, Seoul, Korea
B. Hong, H. Kim, J.H. Kim, K.S. Lee, D.H. Moon, S.K. Park, H.B. Rhee, K.S. Sim

Seoul National University, Seoul, Korea
J. Kim

University of Seoul, Seoul, Korea
M. Choi, G. Hahn, I.C. Park

Sungkyunkwan University, Suwon, Korea
S. Choi, Y. Choi, J. Goh, H. Jeong, T.J. Kim, J. Lee, S. Lee

Vilnius University, Vilnius, Lithuania
M. Janulis, D. Martisiute, P. Petrov, T. Sabonis

Centro de Investigacion y de Estudios Avanzados del IPN, Mexico City, Mexico
H. Castilla Valdez[1], A. Sánchez Hernández

Universidad Iberoamericana, Mexico City, Mexico
S. Carrillo Moreno

Universidad Autónoma de San Luis Potosí, San Luis Potosí, Mexico
A. Morelos Pineda

University of Auckland, Auckland, New Zealand
P. Allfrey, R.N.C. Gray, D. Krofcheck

University of Canterbury, Christchurch, New Zealand
N. Bernardino Rodrigues, P.H. Butler, T. Signal, J.C. Williams

National Centre for Physics, Quaid-I-Azam University, Islamabad, Pakistan
M. Ahmad, I. Ahmed, W. Ahmed, M.I. Asghar, M.I.M. Awan, H.R. Hoorani, I. Hussain, W.A. Khan, T. Khurshid, S. Muhammad, S. Qazi, H. Shahzad

Institute of Experimental Physics, Warsaw, Poland
M. Cwiok, R. Dabrowski, W. Dominik, K. Doroba, M. Konecki, J. Krolikowski, K. Pozniak[16], R. Romaniuk, W. Zabolotny[16], P. Zych

Soltan Institute for Nuclear Studies, Warsaw, Poland
T. Frueboes, R. Gokieli, L. Goscilo, M. Górski, M. Kazana, K. Nawrocki, M. Szleper, G. Wrochna, P. Zalewski

Laboratório de Instrumentação e Física Experimental de Partículas, Lisboa, Portugal
N. Almeida, L. Antunes Pedro, P. Bargassa, A. David, P. Faccioli, P.G. Ferreira Parracho, M. Freitas Ferreira, M. Gallinaro, M. Guerra Jordao, P. Martins, G. Mini, P. Musella, J. Pela, L. Raposo, P.Q. Ribeiro, S. Sampaio, J. Seixas, J. Silva, P. Silva, D. Soares, M. Sousa, J. Varela, H.K. Wöhri

Joint Institute for Nuclear Research, Dubna, Russia
I. Altsybeev, I. Belotelov, P. Bunin, Y. Ershov, I. Filozova, M. Finger, M. Finger Jr., A. Golunov, I. Golutvin, N. Gorbounov, V. Kalagin, A. Kamenev, V. Karjavin, V. Konoplyanikov, V. Korenkov, G. Kozlov, A. Kurenkov, A. Lanev, A. Makankin, V.V. Mitsyn, P. Moisenz, E. Nikonov, D. Oleynik, V. Palichik, V. Perelygin, A. Petrosyan, R. Semenov, S. Shmatov, V. Smirnov, D. Smolin, E. Tikhonenko, S. Vasil'ev, A. Vishnevskiy, A. Volodko, A. Zarubin, V. Zhiltsov

Petersburg Nuclear Physics Institute, Gatchina (St Petersburg), Russia
N. Bondar, L. Chtchipounov, A. Denisov, Y. Gavrikov, G. Gavrilov, V. Golovtsov, Y. Ivanov, V. Kim, V. Kozlov, P. Levchenko, G. Obrant, E. Orishchin, A. Petrunin, Y. Shcheglov, A. Shchetkovskiy, V. Sknar, I. Smirnov, V. Sulimov, V. Tarakanov, L. Uvarov, S. Vavilov, G. Velichko, S. Volkov, A. Vorobyev

Institute for Nuclear Research, Moscow, Russia
Yu. Andreev, A. Anisimov, P. Antipov, A. Dermenev, S. Gninenko, N. Golubev, M. Kirsanov, N. Krasnikov, V. Matveev, A. Pashenkov, V.E. Postoev, A. Solovey, A. Solovey, A. Toropin, S. Troitsky

Institute for Theoretical and Experimental Physics, Moscow, Russia
A. Baud, V. Epshteyn, V. Gavrilov, N. Ilina, V. Kaftanov†, V. Kolosov, M. Kossov[1], A. Krokhotin, S. Kuleshov, A. Oulianov, G. Safronov, S. Semenov, I. Shreyber, V. Stolin, E. Vlasov, A. Zhokin

Moscow State University, Moscow, Russia
E. Boos, M. Dubinin[17], L. Dudko, A. Ershov, A. Gribushin, V. Klyukhin, O. Kodolova, I. Lokhtin, S. Petrushanko, L. Sarycheva, V. Savrin, A. Snigirev, I. Vardanyan

P.N. Lebedev Physical Institute, Moscow, Russia
I. Dremin, M. Kirakosyan, N. Konovalova, S.V. Rusakov, A. Vinogradov

State Research Center of Russian Federation, Institute for High Energy Physics, Protvino, Russia
S. Akimenko, A. Artamonov, I. Azhgirey, S. Bitioukov, V. Burtovoy, V. Grishin[1], V. Kachanov, D. Konstantinov, V. Krychkine, A. Levine, I. Lobov, V. Lukanin, Y. Mel'nik, V. Petrov, R. Ryutin, S. Slabospitsky, A. Sobol, A. Sytine, L. Tourtchanovitch, S. Troshin, N. Tyurin, A. Uzunian, A. Volkov

Vinca Institute of Nuclear Sciences, Belgrade, Serbia
P. Adzic, M. Djordjevic, D. Jovanovic[18], D. Krpic[18], D. Maletic, J. Puzovic[18], N. Smiljkovic

Centro de Investigaciones Energéticas Medioambientales y Tecnológicas (CIEMAT), Madrid, Spain
M. Aguilar-Benitez, J. Alberdi, J. Alcaraz Maestre, P. Arce, J.M. Barcala, C. Battilana, C. Burgos Lazaro, J. Caballero Bejar, E. Calvo, M. Cardenas Montes, M. Cepeda, M. Cerrada, M. Chamizo Llatas, F. Clemente, N. Colino, M. Daniel, B. De La Cruz, A. Delgado Peris, C. Diez Pardos, C. Fernandez Bedoya, J.P. Fernández Ramos, A. Ferrando, J. Flix, M.C. Fouz, P. Garcia-Abia, A.C. Garcia-Bonilla, O. Gonzalez Lopez, S. Goy Lopez, J.M. Hernandez, M.I. Josa, J. Marin, G. Merino, J. Molina, A. Molinero, J.J. Navarrete, J.C. Oller, J. Puerta Pelayo, L. Romero, J. Santaolalla, C. Villanueva Munoz, C. Willmott, C. Yuste

Universidad Autónoma de Madrid, Madrid, Spain
C. Albajar, M. Blanco Otano, J.F. de Trocóniz, A. Garcia Raboso, J.O. Lopez Berengueres

Universidad de Oviedo, Oviedo, Spain
J. Cuevas, J. Fernandez Menendez, I. Gonzalez Caballero, L. Lloret Iglesias, H. Naves Sordo, J.M. Vizan Garcia

Instituto de Física de Cantabria (IFCA), CSIC-Universidad de Cantabria, Santander, Spain
I.J. Cabrillo, A. Calderon, S.H. Chuang, I. Diaz Merino, C. Diez Gonzalez, J. Duarte Campderros, M. Fernandez, G. Gomez, J. Gonzalez Sanchez, R. Gonzalez Suarez, C. Jorda, P. Lobelle Pardo, A. Lopez Virto, J. Marco, R. Marco, C. Martinez Rivero, P. Martinez Ruiz del Arbol, F. Matorras, T. Rodrigo, A. Ruiz Jimeno, L. Scodellaro, M. Sobron Sanudo, I. Vila, R. Vilar Cortabitarte

CERN, European Organization for Nuclear Research, Geneva, Switzerland
D. Abbaneo, E. Albert, M. Alidra, S. Ashby, E. Auffray, J. Baechler, P. Baillon, A.H. Ball, S.L. Bally, D. Barney, F. Beaudette[19], R. Bellan, D. Benedetti, G. Benelli, C. Bernet, P. Bloch, S. Bolognesi, M. Bona, J. Bos, N. Bourgeois, T. Bourrel, H. Breuker, K. Bunkowski, D. Campi, T. Camporesi, E. Cano, A. Cattai, J.P. Chatelain, M. Chauvey, T. Christiansen, J.A. Coarasa Perez, A. Conde Garcia, R. Covarelli, B. Curé, A. De Roeck, V. Delachenal, D. Deyrail, S. Di Vincenzo[20], S. Dos Santos, T. Dupont, L.M. Edera, A. Elliott-Peisert, M. Eppard, M. Favre, N. Frank, W. Funk, A. Gaddi, M. Gastal, M. Gateau, H. Gerwig, D. Gigi, K. Gill, D. Giordano, J.P. Girod, F. Glege, R. Gomez-Reino Garrido, R. Goudard, S. Gowdy, R. Guida, L. Guiducci, J. Gutleber, M. Hansen, C. Hartl, J. Harvey, B. Hegner, H.F. Hoffmann, A. Holzner, A. Honma, M. Huhtinen, V. Innocente, P. Janot, G. Le Godec, P. Lecoq, C. Leonidopoulos, R. Loos, C. Lourenço, A. Lyonnet, A. Macpherson, N. Magini, J.D. Maillefaud, G. Maire, T. Mäki, L. Malgeri, M. Mannelli, L. Masetti, F. Meijers, P. Meridiani, S. Mersi, E. Meschi, A. Meynet Cordonnier, R. Moser, M. Mulders, J. Mulon, M. Noy, A. Oh, G. Olesen, A. Onnela, T. Orimoto, L. Orsini, E. Perez, G. Perinic, J.F. Pernot, P. Petagna, P. Petiot, A. Petrilli, A. Pfeiffer, M. Pierini, M. Pimiä, R. Pintus, B. Pirollet, H. Postema, A. Racz, S. Ravat, S.B. Rew, J. Rodrigues Antunes,

G. Rolandi[21], M. Rovere, V. Ryjov, H. Sakulin, D. Samyn, H. Sauce, C. Schäfer, W.D. Schlatter, M. Schröder, C. Schwick, A. Sciaba, I. Segoni, A. Sharma, N. Siegrist, P. Siegrist, N. Sinanis, T. Sobrier, P. Sphicas[22], D. Spiga, M. Spiropulu[17], F. Stöckli, P. Traczyk, P. Tropea, J. Troska, A. Tsirou, L. Veillet, G.I. Veres, M. Voutilainen, P. Wertelaers, M. Zanetti

Paul Scherrer Institut, Villigen, Switzerland
W. Bertl, K. Deiters, W. Erdmann, K. Gabathuler, R. Horisberger, Q. Ingram, H.C. Kaestli, S. König, D. Kotlinski, U. Langenegger, F. Meier, D. Renker, T. Rohe, J. Sibille[23], A. Starodumov[24]

Institute for Particle Physics, ETH Zurich, Zurich, Switzerland
B. Betev, L. Caminada[25], Z. Chen, S. Cittolin, D.R. Da Silva Di Calafiori, S. Dambach[25], G. Dissertori, M. Dittmar, C. Eggel[25], J. Eugster, G. Faber, K. Freudenreich, C. Grab, A. Hervé, W. Hintz, P. Lecomte, P.D. Luckey, W. Lustermann, C. Marchica[25], P. Milenovic[26], F. Moortgat, A. Nardulli, F. Nessi-Tedaldi, L. Pape, F. Pauss, T. Punz, A. Rizzi, F.J. Ronga, L. Sala, A.K. Sanchez, M.-C. Sawley, V. Sordini, B. Stieger, L. Tauscher†, A. Thea, K. Theofilatos, D. Treille, P. Trüb[25], M. Weber, L. Wehrli, J. Weng, S. Zelepoukine[27]

Universität Zürich, Zurich, Switzerland
C. Amsler, V. Chiochia, S. De Visscher, C. Regenfus, P. Robmann, T. Rommerskirchen, A. Schmidt, D. Tsirigkas, L. Wilke

National Central University, Chung-Li, Taiwan
Y.H. Chang, E.A. Chen, W.T. Chen, A. Go, C.M. Kuo, S.W. Li, W. Lin

National Taiwan University (NTU), Taipei, Taiwan
P. Bartalini, P. Chang, Y. Chao, K.F. Chen, W.-S. Hou, Y. Hsiung, Y.J. Lei, S.W. Lin, R.-S. Lu, J. Schümann, J.G. Shiu, Y.M. Tzeng, K. Ueno, Y. Velikzhanin, C.C. Wang, M. Wang

Cukurova University, Adana, Turkey
A. Adiguzel, A. Ayhan, A. Azman Gokce, M.N. Bakirci, S. Cerci, I. Dumanoglu, E. Eskut, S. Girgis, E. Gurpinar, I. Hos, T. Karaman, T. Karaman, A. Kayis Topaksu, P. Kurt, G. Önengüt, G. Önengüt Gökbulut, K. Ozdemir, S. Ozturk, A. Polatöz, K. Sogut[28], B. Tali, H. Topakli, D. Uzun, L.N. Vergili, M. Vergili

Middle East Technical University, Physics Department, Ankara, Turkey
I.V. Akin, T. Aliev, S. Bilmis, M. Deniz, H. Gamsizkan, A.M. Guler, K. Öcalan, M. Serin, R. Sever, U.E. Surat, M. Zeyrek

Bogaziçi University, Department of Physics, Istanbul, Turkey
M. Deliomeroglu, D. Demir[29], E. Gülmez, A. Halu, B. Isildak, M. Kaya[30], O. Kaya[30], S. Ozkorucuklu[31], N. Sonmez[32]

National Scientific Center, Kharkov Institute of Physics and Technology, Kharkov, Ukraine
L. Levchuk, S. Lukyanenko, D. Soroka, S. Zub

University of Bristol, Bristol, United Kingdom
F. Bostock, J.J. Brooke, T.L. Cheng, D. Cussans, R. Frazier, J. Goldstein, N. Grant, M. Hansen, G.P. Heath, H.F. Heath, C. Hill, B. Huckvale, J. Jackson, C.K. Mackay, S. Metson, D.M. Newbold[33], K. Nirunpong, V.J. Smith, J. Velthuis, R. Walton

Rutherford Appleton Laboratory, Didcot, United Kingdom
K.W. Bell, C. Brew, R.M. Brown, B. Camanzi, D.J.A. Cockerill, J.A. Coughlan, N.I. Geddes, K. Harder, S. Harper, B.W. Kennedy, P. Murray, C.H. Shepherd-Themistocleous, I.R. Tomalin, J.H. Williams†, W.J. Womersley, S.D. Worm

Imperial College, University of London, London, United Kingdom
R. Bainbridge, G. Ball, J. Ballin, R. Beuselinck, O. Buchmuller, D. Colling, N. Cripps, G. Davies, M. Della Negra, C. Foudas, J. Fulcher, D. Futyan, G. Hall, J. Hays, G. Iles, G. Karapostoli, B.C. MacEvoy, A.-M. Magnan, J. Marrouche, J. Nash, A. Nikitenko[24], A. Papageorgiou, M. Pesaresi, K. Petridis, M. Pioppi[34], D.M. Raymond, N. Rompotis, A. Rose, M.J. Ryan, C. Seez, P. Sharp, G. Sidiropoulos[1], M. Stettler, M. Stoye, M. Takahashi, A. Tapper, C. Timlin, S. Tourneur, M. Vazquez Acosta, T. Virdee[1], S. Wakefield, D. Wardrope, T. Whyntie, M. Wingham

Brunel University, Uxbridge, United Kingdom
J.E. Cole, I. Goitom, P.R. Hobson, A. Khan, P. Kyberd, D. Leslie, C. Munro, I.D. Reid, C. Siamitros, R. Taylor, L. Teodorescu, I. Yaselli

Boston University, Boston, USA
T. Bose, M. Carleton, E. Hazen, A.H. Heering, A. Heister, J. St. John, P. Lawson, D. Lazic, D. Osborne, J. Rohlf, L. Sulak, S. Wu

Brown University, Providence, USA
J. Andrea, A. Avetisyan, S. Bhattacharya, J.P. Chou, D. Cutts, S. Esen, G. Kukartsev, G. Landsberg, M. Narain, D. Nguyen, T. Speer, K.V. Tsang

University of California, Davis, Davis, USA
R. Breedon, M. Calderon De La Barca Sanchez, M. Case, D. Cebra, M. Chertok, J. Conway, P.T. Cox, J. Dolen, R. Erbacher, E. Friis, W. Ko, A. Kopecky, R. Lander, A. Lister, H. Liu, S. Maruyama, T. Miceli, M. Nikolic, D. Pellett, J. Robles, M. Searle, J. Smith, M. Squires, J. Stilley, M. Tripathi, R. Vasquez Sierra, C. Veelken

University of California, Los Angeles, Los Angeles, USA
V. Andreev, K. Arisaka, D. Cline, R. Cousins, S. Erhan[1], J. Hauser, M. Ignatenko, C. Jarvis, J. Mumford, C. Plager, G. Rakness, P. Schlein[†], J. Tucker, V. Valuev, R. Wallny, X. Yang

University of California, Riverside, Riverside, USA
J. Babb, M. Bose, A. Chandra, R. Clare, J.A. Ellison, J.W. Gary, G. Hanson, G.Y. Jeng, S.C. Kao, F. Liu, H. Liu, A. Luthra, H. Nguyen, G. Pasztor[35], A. Satpathy, B.C. Shen[†], R. Stringer, J. Sturdy, V. Sytnik, R. Wilken, S. Wimpenny

University of California, San Diego, La Jolla, USA
J.G. Branson, E. Dusinberre, D. Evans, F. Golf, R. Kelley, M. Lebourgeois, J. Letts, E. Lipeles, B. Mangano, J. Muelmenstaedt, M. Norman, S. Padhi, A. Petrucci, H. Pi, M. Pieri, R. Ranieri, M. Sani, V. Sharma, S. Simon, F. Würthwein, A. Yagil

University of California, Santa Barbara, Santa Barbara, USA
C. Campagnari, M. D'Alfonso, T. Danielson, J. Garberson, J. Incandela, C. Justus, P. Kalavase, S.A. Koay, D. Kovalskyi, V. Krutelyov, J. Lamb, S. Lowette, V. Pavlunin, F. Rebassoo, J. Ribnik, J. Richman, R. Rossin, D. Stuart, W. To, J.R. Vlimant, M. Witherell

California Institute of Technology, Pasadena, USA
A. Apresyan, A. Bornheim, J. Bunn, M. Chiorboli, M. Gataullin, D. Kcira, V. Litvine, Y. Ma, H.B. Newman, C. Rogan, V. Timciuc, J. Veverka, R. Wilkinson, Y. Yang, L. Zhang, K. Zhu, R.Y. Zhu

Carnegie Mellon University, Pittsburgh, USA
B. Akgun, R. Carroll, T. Ferguson, D.W. Jang, S.Y. Jun, M. Paulini, J. Russ, N. Terentyev, H. Vogel, I. Vorobiev

University of Colorado at Boulder, Boulder, USA
J.P. Cumalat, M.E. Dinardo, B.R. Drell, W.T. Ford, B. Heyburn, E. Luiggi Lopez, U. Nauenberg, K. Stenson, K. Ulmer, S.R. Wagner, S.L. Zang

Cornell University, Ithaca, USA
L. Agostino, J. Alexander, F. Blekman, D. Cassel, A. Chatterjee, S. Das, L.K. Gibbons, B. Heltsley, W. Hopkins, A. Khukhunaishvili, B. Kreis, V. Kuznetsov, J.R. Patterson, D. Puigh, A. Ryd, X. Shi, S. Stroiney, W. Sun, W.D. Teo, J. Thom, J. Vaughan, Y. Weng, P. Wittich

Fairfield University, Fairfield, USA
C.P. Beetz, G. Cirino, C. Sanzeni, D. Winn

Fermi National Accelerator Laboratory, Batavia, USA
S. Abdullin, M.A. Afaq[1], M. Albrow, B. Ananthan, G. Apollinari, M. Atac, W. Badgett, L. Bagby, J.A. Bakken, B. Baldin, S. Banerjee, K. Banicz, L.A.T. Bauerdick, A. Beretvas, J. Berryhill, P.C. Bhat, K. Biery, M. Binkley, I. Bloch, F. Borcherding, A.M. Brett, K. Burkett, J.N. Butler, V. Chetluru, H.W.K. Cheung, F. Chlebana, I. Churin, S. Cihangir, M. Crawford, W. Dagenhart, M. Demarteau, G. Derylo, D. Dykstra, D.P. Eartly, J.E. Elias, V.D. Elvira, D. Evans, L. Feng, M. Fischler, I. Fisk, S. Foulkes, J. Freeman, P. Gartung, E. Gottschalk, T. Grassi, D. Green, Y. Guo, O. Gutsche, A. Hahn, J. Hanlon, R.M. Harris, B. Holzman, J. Howell, D. Hufnagel, E. James, H. Jensen, M. Johnson, C.D. Jones, U. Joshi, E. Juska, J. Kaiser, B. Klima, S. Kossiakov, K. Kousouris, S. Kwan, C.M. Lei, P. Limon, J.A. Lopez Perez, S. Los, L. Lueking, G. Lukhanin, S. Lusin[1], J. Lykken, K. Maeshima, J.M. Marraffino, D. Mason, P. McBride, T. Miao, K. Mishra, S. Moccia, R. Mommsen, S. Mrenna, A.S. Muhammad, C. Newman-Holmes, C. Noeding, V. O'Dell, O. Prokofyev, R. Rivera, C.H. Rivetta, A. Ronzhin, P. Rossman, S. Ryu, V. Sekhri, E. Sexton-Kennedy, I. Sfiligoi, S. Sharma, T.M. Shaw, D. Shpakov, E. Skup, R.P. Smith[†], A. Soha, W.J. Spalding, L. Spiegel, I. Suzuki, P. Tan, W. Tanenbaum, S. Tkaczyk[1], R. Trentadue[1], L. Uplegger, E.W. Vaandering, R. Vidal, J. Whitmore, E. Wicklund, W. Wu, J. Yarba, F. Yumiceva, J.C. Yun

University of Florida, Gainesville, USA
D. Acosta, P. Avery, V. Barashko, D. Bourilkov, M. Chen, G.P. Di Giovanni, D. Dobur, A. Drozdetskiy, R.D. Field, Y. Fu, I.K. Furic, J. Gartner, D. Holmes, B. Kim, S. Klimenko, J. Konigsberg, A. Korytov, K. Kotov, A. Kropivnitskaya, T. Kypreos, A. Madorsky, K. Matchev, G. Mitselmakher, Y. Pakhotin, J. Piedra Gomez, C. Prescott, V. Rapsevicius, R. Remington, M. Schmitt, B. Scurlock, D. Wang, J. Yelton

Florida International University, Miami, USA
C. Ceron, V. Gaultney, L. Kramer, L.M. Lebolo, S. Linn, P. Markowitz, G. Martinez, J.L. Rodriguez

Florida State University, Tallahassee, USA
T. Adams, A. Askew, H. Baer, M. Bertoldi, J. Chen, W.G.D. Dharmaratna, S.V. Gleyzer, J. Haas, S. Hagopian, V. Hagopian, M. Jenkins, K.F. Johnson, E. Prettner, H. Prosper, S. Sekmen

Florida Institute of Technology, Melbourne, USA
M.M. Baarmand, S. Guragain, M. Hohlmann, H. Kalakhety, H. Mermerkaya, R. Ralich, I. Vodopiyanov

University of Illinois at Chicago (UIC), Chicago, USA
B. Abelev, M.R. Adams, I.M. Anghel, L. Apanasevich, V.E. Bazterra, R.R. Betts, J. Callner, M.A. Castro, R. Cavanaugh, C. Dragoiu, E.J. Garcia-Solis, C.E. Gerber, D.J. Hofman, S. Khalatian, C. Mironov, E. Shabalina, A. Smoron, N. Varelas

The University of Iowa, Iowa City, USA
U. Akgun, E.A. Albayrak, A.S. Ayan, B. Bilki, R. Briggs, K. Cankocak[36], K. Chung, W. Clarida, P. Debbins, F. Duru, F.D. Ingram, C.K. Lae, E. McCliment, J.-P. Merlo, A. Mestvirishvili, M.J. Miller, A. Moeller, J. Nachtman, C.R. Newsom, E. Norbeck, J. Olson, Y. Onel, F. Ozok, J. Parsons, I. Schmidt, S. Sen, J. Wetzel, T. Yetkin, K. Yi

Johns Hopkins University, Baltimore, USA
B.A. Barnett, B. Blumenfeld, A. Bonato, C.Y. Chien, D. Fehling, G. Giurgiu, A.V. Gritsan, Z.J. Guo, P. Maksimovic, S. Rappoccio, M. Swartz, N.V. Tran, Y. Zhang

The University of Kansas, Lawrence, USA
P. Baringer, A. Bean, O. Grachov, M. Murray, V. Radicci, S. Sanders, J.S. Wood, V. Zhukova

Kansas State University, Manhattan, USA
D. Bandurin, T. Bolton, K. Kaadze, A. Liu, Y. Maravin, D. Onoprienko, I. Svintradze, Z. Wan

Lawrence Livermore National Laboratory, Livermore, USA
J. Gronberg, J. Hollar, D. Lange, D. Wright

University of Maryland, College Park, USA
D. Baden, R. Bard, M. Boutemeur, S.C. Eno, D. Ferencek, N.J. Hadley, R.G. Kellogg, M. Kirn, S. Kunori, K. Rossato, P. Rumerio, F. Santanastasio, A. Skuja, J. Temple, M.B. Tonjes, S.C. Tonwar, T. Toole, E. Twedt

Massachusetts Institute of Technology, Cambridge, USA
B. Alver, G. Bauer, J. Bendavid, W. Busza, E. Butz, I.A. Cali, M. Chan, D. D'Enterria, P. Everaerts, G. Gomez Ceballos, K.A. Hahn, P. Harris, S. Jaditz, Y. Kim, M. Klute, Y.-J. Lee, W. Li, C. Loizides, T. Ma, M. Miller, S. Nahn, C. Paus, C. Roland, G. Roland, M. Rudolph, G. Stephans, K. Sumorok, K. Sung, S. Vaurynovich, E.A. Wenger, B. Wyslouch, S. Xie, Y. Yilmaz, A.S. Yoon

University of Minnesota, Minneapolis, USA
D. Bailleux, S.I. Cooper, P. Cushman, B. Dahmes, A. De Benedetti, A. Dolgopolov, P.R. Dudero, R. Egeland, G. Franzoni, J. Haupt, A. Inyakin[37], K. Klapoetke, Y. Kubota, J. Mans, N. Mirman, D. Petyt, V. Rekovic, R. Rusack, M. Schroeder, A. Singovsky, J. Zhang

University of Mississippi, University, USA
L.M. Cremaldi, R. Godang, R. Kroeger, L. Perera, R. Rahmat, D.A. Sanders, P. Sonnek, D. Summers

University of Nebraska-Lincoln, Lincoln, USA
K. Bloom, B. Bockelman, S. Bose, J. Butt, D.R. Claes, A. Dominguez, M. Eads, J. Keller, T. Kelly, I. Kravchenko, J. Lazo-Flores, C. Lundstedt, H. Malbouisson, S. Malik, G.R. Snow

State University of New York at Buffalo, Buffalo, USA
U. Baur, I. Iashvili, A. Kharchilava, A. Kumar, K. Smith, M. Strang

Northeastern University, Boston, USA
G. Alverson, E. Barberis, O. Boeriu, G. Eulisse, G. Govi, T. McCauley, Y. Musienko[38], S. Muzaffar, I. Osborne, T. Paul, S. Reucroft, J. Swain, L. Taylor, L. Tuura

Northwestern University, Evanston, USA
A. Anastassov, B. Gobbi, A. Kubik, R.A. Ofierzynski, A. Pozdnyakov, M. Schmitt, S. Stoynev, M. Velasco, S. Won

University of Notre Dame, Notre Dame, USA
L. Antonelli, D. Berry, M. Hildreth, C. Jessop, D.J. Karmgard, T. Kolberg, K. Lannon, S. Lynch,

N. Marinelli, D.M. Morse, R. Ruchti, J. Slaunwhite, J. Warchol, M. Wayne

The Ohio State University, Columbus, USA
B. Bylsma, L.S. Durkin, J. Gilmore[39], J. Gu, P. Killewald, T.Y. Ling, G. Williams

Princeton University, Princeton, USA
N. Adam, E. Berry, P. Elmer, A. Garmash, D. Gerbaudo, V. Halyo, A. Hunt, J. Jones, E. Laird, D. Marlow, T. Medvedeva, M. Mooney, J. Olsen, P. Piroué, D. Stickland, C. Tully, J.S. Werner, T. Wildish, Z. Xie, A. Zuranski

University of Puerto Rico, Mayaguez, USA
J.G. Acosta, M. Bonnett Del Alamo, X.T. Huang, A. Lopez, H. Mendez, S. Oliveros, J.E. Ramirez Vargas, N. Santacruz, A. Zatzerklyany

Purdue University, West Lafayette, USA
E. Alagoz, E. Antillon, V.E. Barnes, G. Bolla, D. Bortoletto, A. Everett, A.F. Garfinkel, Z. Gecse, L. Gutay, N. Ippolito, M. Jones, O. Koybasi, A.T. Laasanen, N. Leonardo, C. Liu, V. Maroussov, P. Merkel, D.H. Miller, N. Neumeister, A. Sedov, I. Shipsey, H.D. Yoo, Y. Zheng

Purdue University Calumet, Hammond, USA
P. Jindal, N. Parashar

Rice University, Houston, USA
V. Cuplov, K.M. Ecklund, F.J.M. Geurts, J.H. Liu, D. Maronde, M. Matveev, B.P. Padley, R. Redjimi, J. Roberts, L. Sabbatini, A. Tumanov

University of Rochester, Rochester, USA
B. Betchart, A. Bodek, H. Budd, Y.S. Chung, P. de Barbaro, R. Demina, H. Flacher, Y. Gotra, A. Harel, S. Korjenevski, D.C. Miner, D. Orbaker, G. Petrillo, D. Vishnevskiy, M. Zielinski

The Rockefeller University, New York, USA
A. Bhatti, L. Demortier, K. Goulianos, K. Hatakeyama, G. Lungu, C. Mesropian, M. Yan

Rutgers, the State University of New Jersey, Piscataway, USA
O. Atramentov, E. Bartz, Y. Gershtein, E. Halkiadakis, D. Hits, A. Lath, K. Rose, S. Schnetzer, S. Somalwar, R. Stone, S. Thomas, T.L. Watts

University of Tennessee, Knoxville, USA
G. Cerizza, M. Hollingsworth, S. Spanier, Z.C. Yang, A. York

Texas A&M University, College Station, USA
J. Asaadi, A. Aurisano, R. Eusebi, A. Golyash, A. Gurrola, T. Kamon, C.N. Nguyen, J. Pivarski, A. Safonov, S. Sengupta, D. Toback, M. Weinberger

Texas Tech University, Lubbock, USA
N. Akchurin, L. Berntzon, K. Gumus, C. Jeong, H. Kim, S.W. Lee, S. Popescu, Y. Roh, A. Sill, I. Volobouev, E. Washington, R. Wigmans, E. Yazgan

Vanderbilt University, Nashville, USA
D. Engh, C. Florez, W. Johns, S. Pathak, P. Sheldon

University of Virginia, Charlottesville, USA
D. Andelin, M.W. Arenton, M. Balazs, S. Boutle, M. Buehler, S. Conetti, B. Cox, R. Hirosky, A. Ledovskoy, C. Neu, D. Phillips II, M. Ronquest, R. Yohay

Wayne State University, Detroit, USA
S. Gollapinni, K. Gunthoti, R. Harr, P.E. Karchin, M. Mattson, A. Sakharov

University of Wisconsin, Madison, USA
M. Anderson, M. Bachtis, J.N. Bellinger, D. Carlsmith, I. Crotty[1], S. Dasu, S. Dutta, J. Efron, F. Feyzi, K. Flood, L. Gray, K.S. Grogg, M. Grothe, R. Hall-Wilton[1], M. Jaworski, P. Klabbers, J. Klukas, A. Lanaro, C. Lazaridis, J. Leonard, R. Loveless, M. Magrans de Abril, A. Mohapatra, G. Ott, G. Polese, D. Reeder, A. Savin, W.H. Smith, A. Sourkov[40], J. Swanson, M. Weinberg, D. Wenman, M. Wensveen, A. White

†: Deceased
1: Also at CERN, European Organization for Nuclear Research, Geneva, Switzerland
2: Also at Universidade Federal do ABC, Santo Andre, Brazil
3: Also at Soltan Institute for Nuclear Studies, Warsaw, Poland
4: Also at Université de Haute-Alsace, Mulhouse, France
5: Also at Centre de Calcul de l'Institut National de Physique Nucleaire et de Physique des Particules (IN2P3), Villeurbanne, France
6: Also at Moscow State University, Moscow, Russia
7: Also at Institute of Nuclear Research ATOMKI, Debrecen, Hungary
8: Also at University of California, San Diego, La Jolla, USA
9: Also at Tata Institute of Fundamental Research - HECR, Mumbai, India
10: Also at University of Visva-Bharati, Santiniketan, India
11: Also at Facolta' Ingegneria Universita' di Roma "La Sapienza", Roma, Italy
12: Also at Università della Basilicata, Potenza, Italy
13: Also at Laboratori Nazionali di Legnaro dell' INFN, Legnaro, Italy
14: Also at Università di Trento, Trento, Italy
15: Also at ENEA - Casaccia Research Center, S. Maria di Galeria, Italy
16: Also at Warsaw University of Technology, Institute of Electronic Systems, Warsaw, Poland
17: Also at California Institute of Technology, Pasadena, USA
18: Also at Faculty of Physics of University of Belgrade, Belgrade, Serbia
19: Also at Laboratoire Leprince-Ringuet, Ecole Polytechnique, IN2P3-CNRS, Palaiseau, France
20: Also at Alstom Contracting, Geneve, Switzerland
21: Also at Scuola Normale e Sezione dell' INFN, Pisa, Italy
22: Also at University of Athens, Athens, Greece
23: Also at The University of Kansas, Lawrence, USA
24: Also at Institute for Theoretical and Experimental Physics, Moscow, Russia
25: Also at Paul Scherrer Institut, Villigen, Switzerland
26: Also at Vinca Institute of Nuclear Sciences, Belgrade, Serbia
27: Also at University of Wisconsin, Madison, USA
28: Also at Mersin University, Mersin, Turkey
29: Also at Izmir Institute of Technology, Izmir, Turkey
30: Also at Kafkas University, Kars, Turkey
31: Also at Suleyman Demirel University, Isparta, Turkey
32: Also at Ege University, Izmir, Turkey
33: Also at Rutherford Appleton Laboratory, Didcot, United Kingdom
34: Also at INFN Sezione di Perugia; Universita di Perugia, Perugia, Italy
35: Also at KFKI Research Institute for Particle and Nuclear Physics, Budapest, Hungary
36: Also at Istanbul Technical University, Istanbul, Turkey
37: Also at University of Minnesota, Minneapolis, USA
38: Also at Institute for Nuclear Research, Moscow, Russia
39: Also at Texas A&M University, College Station, USA
40: Also at State Research Center of Russian Federation, Institute for High Energy Physics, Protvino, Russia